

A SURVEY OF ATOMIC CARBON AT HIGH REDSHIFT

F. WALTER¹, A. WEISS², D. DOWNES³, R. DECARLI¹, C. HENKEL²

Draft version November 11, 2018

ABSTRACT

We present a survey of atomic carbon (C I) emission in high-redshift ($z > 2$) submillimeter galaxies (SMGs) and quasar host galaxies (QSOs). Sensitive observations of the C I($^3P_1 \rightarrow ^3P_0$) and C I($^3P_2 \rightarrow ^3P_1$) lines have been obtained at the IRAM Plateau de Bure interferometer and the IRAM 30 m telescope. A total of 16 C I lines have been targeted in 10 sources, leading to a total of 10 detected lines — this doubles the number of C I observations at high redshift to date. We include previously published C I observations (an additional 5 detected sources) in our analysis. Our main finding is that the C I properties of high-redshift systems do not differ significantly from what is found in low-redshift systems, including the Milky Way. The C I($^3P_2 \rightarrow ^3P_1$)/C I($^3P_1 \rightarrow ^3P_0$) and the C I($^3P_1 \rightarrow ^3P_0$)/ $^{12}\text{CO}(3-2)$ line luminosity (L') ratios change little in our sample, with respective ratios of 0.55 ± 0.15 and 0.32 ± 0.13 . The C I lines are not an important contributor to cooling of the molecular gas (average $L_{\text{C I}}/L_{\text{FIR}} \sim (7.7 \pm 4.6) \times 10^{-6}$). We derive a mean carbon excitation temperature of 29.1 ± 6.3 K, broadly consistent with dust temperatures derived for high-redshift starforming systems, but lower than gas temperatures typically derived for starbursts in the local universe. The carbon abundance of $X[\text{C I}]/X[\text{H}_2] \sim (8.4 \pm 3.5) \times 10^{-5}$ is of the same order as found in the Milky Way and nearby galaxies. This implies that the high- z galaxies studied here are significantly enriched in carbon on galactic scales, even though the look-back times are considerable (the average redshift of the sample sources corresponds to an age of the universe of ~ 2 Gyr).

Subject headings: galaxies: formation — cosmology: observations — infrared: galaxies — galaxies: starbursts — galaxies: evolution

1. INTRODUCTION

Detections of carbon monoxide (CO) and dust, in objects at $z > 2$ have enabled studies of the molecular gas properties in the early phases of galaxy formation (e.g., review by Solomon & Vanden Bout 2005). Molecular gas masses $> 10^{10} M_{\odot}$, enriched in C and O, provide strong evidence for powerful starbursts at early epochs in objects that may have later turned into massive spirals and/or elliptical galaxies. Until now, mid- J ($J=3-6$) CO lines and the continuum emission from dust have primarily been used to characterize the physical properties of these massive gas reservoirs. One key approach is to observe the different rotational (J) transitions of CO (so-called ‘CO line spectral energy distribution’, or ‘CO line ladder’) and use radiative transfer models to constrain molecular gas masses, densities, and temperatures (see the compilation by Weiß et al. 2007, 2011, hereafter W11). In such analyses, however, it is frequently found that the density and kinetic temperature of the molecular gas are degenerate, so that data from additional tracers of the gas phase would be highly desirable.

Such an alternative tracer of the cold molecular gas phase is atomic carbon (C I). Studies of atomic carbon in the local universe have been carried out in molecular clouds of the galactic disk, the galactic center, M82 and other nearby galaxies (e.g., White et al. 1994; Stutzki et al. 1997; Gerin & Phillips 1998; 2000; Ojha et al.

2001; Israel & Baas 2002; Schneider et al. 2003, Israel 2005). These studies have shown that C I is closely associated with the CO emission independent of environment. Since the critical density for the C I($1-0$) and $^{12}\text{CO}(J=1 \rightarrow 0)$ lines are both $n_{\text{cr}} \approx 10^3 \text{ cm}^{-3}$, this finding suggests that the transitions arise from the same volume and share similar excitation temperatures (e.g. Ikeda et al. 2002). For reference, the critical densities for the C I($1-0$) and C I($2-1$) lines are $1 \times 10^3 \text{ cm}^{-3}$ and $3 \times 10^3 \text{ cm}^{-3}$, respectively (Schöier et al. 2005)⁴. As pointed out by Papadopoulos et al. (2004) such a close connection between C I and CO was not expected from early theoretical work (Tielens & Hollenbach 1985a, 1985b), where the C I emission was thought to emerge from a narrow C II/C I/CO transition zone in molecular clouds.

Because the ^3P fine-structure system of atomic carbon forms a simple three-level system, detection of both optically thin carbon lines, C I($^3P_1 \rightarrow ^3P_0$) (rest frequency: 492.161 GHz, hereafter C I($1-0$)) and C I($^3P_2 \rightarrow ^3P_1$) (rest frequency: 809.344 GHz, hereafter C I($2-1$)), enables one to derive the excitation temperature, neutral carbon column density and mass independently of any other information (e.g., Ojha et al. 2001, Weiß et al. 2003). A combination of this method (using C I) with the aforementioned CO SEDs is particularly powerful as it eliminates some of the degeneracy frequently found in CO radiative transfer models. Therefore, assuming that C I and CO trace similar volumes on galactic scales, the carbon excitation temperature allows us to pin down the CO excitation conditions, as the excitation temperature of C I and CO($1-0$) are expected to be similar.

¹ Max-Planck-Institut für Astronomie, Königstuhl 17, D-69117 Heidelberg, Germany [e-mail: walter@mpia.de]

² Max-Planck-Institut für Radioastronomie, Auf dem Hügel 69, D-53121 Bonn, Germany

³ Institut de Radio Astronomie Millimétrique (IRAM), St. Martin d’Hères, France

⁴ For details see: <http://www.strw.leidenuniv.nl/~moldata/datafiles/catom.da>

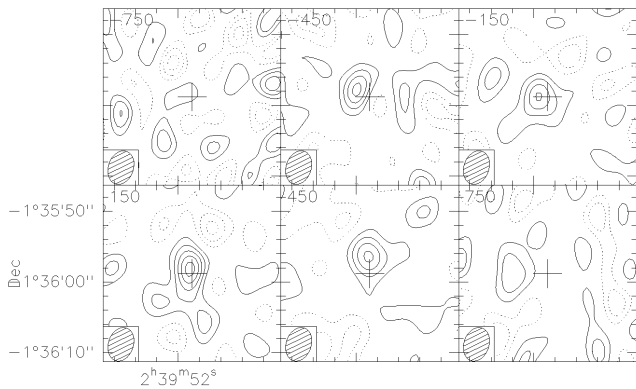


FIG. 1.— $\text{C I}(1-0)$ channel maps of SMM J02399-0136. Each channel is 300 km s^{-1} wide and the central velocity is given in the top left corner. Contours are shown in steps of 1σ ($1\sigma = 0.31 \text{ mJy beam}^{-1}$)

Previous observations of C I at high redshift (see references given in Section 4 and the related Table) have shown that both the $\text{C I}(1-0)$ and $\text{C I}(2-1)$ lines are typically significantly fainter than the respective CO lines at similar frequencies (partly because they are typically optically thin). In this paper we report on observations of atomic carbon towards 10 high-redshift sources (a total of 16 C I lines) that encompass both submillimeter galaxies (SMGs) as well as quasar host galaxies (QSOs). These observations roughly double the number of high- z C I line detections that have been presented in the literature previously (in a dozen papers). In Section 2 we present the observations that have been obtained with the IRAM Plateau de Bure Interferometer (hereafter: PdBI) as well as the IRAM 30 m telescope. In Section 3 we discuss the observations of the individual sources. We compare the C I properties (including sources from the literature) in Section 4. Section 5 summarizes our findings. Throughout this paper we use a Λ cosmology with $H_0 = 71 \text{ km s}^{-1} \text{ Mpc}^{-1}$, $\Omega_\Lambda = 0.73$ and $\Omega_m = 0.27$ (Spergel et al. 2003, 2007).

2. OBSERVATIONS

2.1. Source Selection

Given the expected faintness of the C I emission line we have selected sources that are bright in CO emission. We have mostly targeted quasars using the IRAM 30 m telescope as their linewidths are typically small ($\sim 400 \text{ km s}^{-1}$), to minimize susceptibility to low-frequency baseline instabilities in the single dish observations. We have typically used the (intrinsically more stable) PdBI in the case of the SMGs that are faint and have significant linewidths ($\sim 800 - 1000 \text{ km s}^{-1}$, e.g. Greve et al. 2005). The SMGs have been selected to be in the redshift range $2.03 < z < 2.81$ so that both C I transitions can be observed in the 2 and 1 mm bands of the PdBI and 30 m telescope. As discussed in the individual sources below, some of the SMGs host an AGN, i.e. the two populations that have historically been referred to as SMGs and quasars do overlap. Most of the quasars in our sample have higher redshifts. The source names, coordinates, redshifts, targeted C I transitions and telescopes used are given in Table 1 and results for individual sources are discussed in Section 3.

2.2. IRAM Plateau de Bure Observations

The data were taken in the years 2008 and 2009 (project IDs S046 & S0B3) using the upgraded PdBI with its dual polarization receivers and a bandwidth of 1 GHz (single polarization). At 2 mm, typically five 15m antennas were available in the compact D configuration, with spacings from 24 to 86m. These short spacings had average rms phase errors of 15° at 2 mm and 30° at 1 mm. System temperatures were 150K in the lower sideband at 2 mm, and 250 to 400K in the lower sideband at 1.3mm. The spectral correlators covered $\sim 1500 \text{ km s}^{-1}$ at 2 mm and 1000 km s^{-1} at 1 mm, with instrumental resolutions of 8 and 4 km s^{-1} , respectively. The primary amplitude calibrators were 3C454.3 (variable, but typically 25 Jy at 2 mm and 13 Jy at 1.3mm), and MWC349 (nonvarying, with 1.9 and 1.6 Jy at 2 and 1.3mm). The typical uncertainties in the flux scales and overall calibration are $\sim 10\%$ at 2 mm and $\sim 15-20\%$ at 1.3mm and should be added to the formal fitting errors quoted in the remainder of this paper. The observing program monitored phases every 20 min. The data processing program used water-vapour monitoring receivers at 22 GHz on each antenna to correct amplitudes and phases at 2 mm and 1.3 mm for short-term changes in atmospheric water vapor. All visibilities are weighted by the integration time and the inverse square of the system temperature. Source maps were made with ‘natural weighting’ of the visibilities to maximise the sensitivity. The tuned frequencies, the resulting beam sizes (and position angles), and the 1σ rms over the full bandwidth (1 GHz) for each source are given in Table 2. The primary beam size of PdBI at 2 mm (1 mm) is $\sim 35''$ ($\sim 22''$). Emission has been cleaned to the 1.5σ level in a tight box around the source. In the case of non-detections no cleaning was performed.

2.3. IRAM 30 m Observations

Observations were carried out with the IRAM 30 m telescope in the years 2004–2007. We used the CD or AB receiver configurations with the C/D 150 receivers tuned to the $\text{C I}(1-0)$ transition or the A/B 230 receivers tuned to $\text{C I}(2-1)$. The beam size of the 30 m at 140 GHz (230 GHz) is $\approx 17''$ ($11''$). Typical system temperatures were $\approx 200 \text{ K}$ and $\approx 270 \text{ K}$ during winter and summer respectively. The observations were carried out in wobbler switching mode, with a switching frequency of 0.5 Hz and a wobbler throw of $50''$ in azimuth. Pointing was checked frequently and was found to be stable within $3''$. Calibration was obtained every 12 min using standard hot/cold-load absorber measurements. Both Mars and Uranus were used for calibration. The antenna gain was found to be consistent with the standard value of $6.6 (10) \text{ Jy K}^{-1}$ at 140 (230) GHz (temperatures in units of T_A^*). We estimate the flux density scale to be accurate to about 15%.

Data were recorded using the 4 MHz filter banks on each receiver (512 channels, 1GHz bandwidth, 4 MHz channel spacing) and were processed using the CLASS software. After dropping bad data only linear baselines were subtracted from individual spectra. The tuned frequencies and the noise in each 150 km s^{-1} channel are given in Table 3.

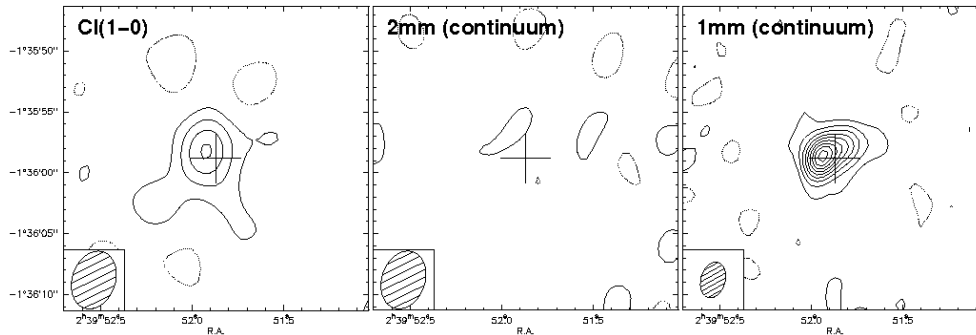


FIG. 2.— Results for SMM J02399–0136. *Left*: Integrated C I(1–0) emission from -500 km s^{-1} to $+500 \text{ km s}^{-1}$, with contours starting at $\pm 2\sigma$ in steps of 2σ ($1\sigma=0.17 \text{ mJy}$). *Middle*: Continuum measurement at 129.2 GHz (line-free channels of the C I(1–0) observations, using the same total bandwidth as for the line), same contouring and 1σ sensitivity as in the left panel. No continuum is detected at 129.2 GHz. *Right*: Continuum emission at 212.5 GHz, with contours starting at $\pm 2\sigma$ in steps of 2σ ($1\sigma=0.18 \text{ mJy}$). The beam sizes are shown in the bottom left corner, respectively (see Table 2).

TABLE 1
PROPERTIES OF OBSERVED TARGETS

source	RA J2000.0	DEC J2000.0	z	FWHM km s^{-1}	transition	telescope	references ^a
SMM J02399–0136	02:38:51.87	–01:35:58.8	2.808	~ 1100	C I(1–0), C I(2–1)	PdBI	1, 2
APM 08279+5255	08:31:41.64	+52:45:17.5	3.911	480 ± 35	C I(2–1)	30 m	3
RX J0911+0551	09:11:27.50	+05:50:52.0	2.796	150 ± 20	C I(1–0), C I(2–1)	30 m	4, 5
SMM J123549+6215 ^b	12:35:49.42	+62:15:36.9	2.202	600 ± 50	C I(1–0), C I(2–1)	PdBI	6
BRI 1335–0417	13:38:03.42	–04:32:34.1	4.407	420 ± 60	C I(2–1)	30 m	7
SMM J14011+0252	14:01:04.93	+02:52:24.1	2.565	190 ± 11	C I(2–1)	30 m	8, 9
SMM J16359+6612	16:35:54.10	+66:12:23.8	2.517	500 ± 100	C I(1–0), C I(2–1)	30 m	10, 11
SMM J163650+4057 ^c	16:36:50.41	+40:57:34.3	2.385	710 ± 50	C I(1–0), C I(2–1)	PdBI	12, 6
SMM J163658+4105 ^d	16:36:58.17	+41:05:23.3	2.452	800 ± 50	C I(1–0), C I(2–1)	PdBI	13, 6
PSS J2322+1944	23:22:07.25	+19:44:22.1	4.120	200 ± 70	C I(2–1)	30 m	14

NOTE. — The coordinates and redshifts refer to the pointing center and redshift used for tuning the receivers. These values are taken from the references given in the last column.

^a references (coordinates, redshifts, FWHM’s) are: [1]: Frayer et al. 1998; [2]: Genzel et al. 2003; [3]: Downes et al. 1999; [4]: Hainline et al. 2004; [5]: W11; [6]: Tacconi et al. 2006; [7]: Guilloteau et al. 1999; [8]: Frayer et al. 1999; [9]: Downes & Solomon 2003; [10]: Sheth et al. 2004; [11]: Kneib et al. 2005, [12]: Neri et al. 2003; [13]: Greve et al. 2005; [14]: Cox et al. 2002.

^b alternative name: HDF 76.

^c alternative name: Elias N2 850.4.

^d alternative name: Elias N2 850.2.

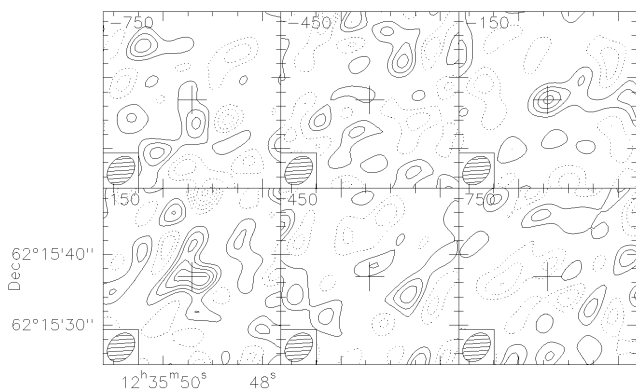


FIG. 3.— C I(1–0) channel maps of SMM J123549+6215. Each channel is 300 km s^{-1} wide and the central velocity is given in the top left corner. Contours are shown in steps of 1σ ($1\sigma=0.43 \text{ mJy beam}^{-1}$)

3. RESULTS

In the following we present the results for each source. The PdBI observations are summarized in Section 3.1 (Figs. 1–6) and the 30 m observations in Section 3.2

(Figs. 7–12).

3.1. PdBI Observations

3.1.1. C I Line Emission

The main results and data analysis are described in the following: C I(1–0) emission (observed at 2 mm wavelength) has been detected at a significant level in three of the four sources that have been targeted. However, C I(2–1) emission (observed at 1 mm wavelengths) has been tentatively detected only in one source (SMM J02399–0136). The latter measurement is complicated by the fact that the faint C I(2–1) emission is situated on top of bright continuum emission at 1 mm wavelengths. An additional complication is that the rest frequency of the CO(7–6) line (806.651 GHz) is close to that of C I(2–1) (809.344 GHz), i.e. the velocity difference at $z\sim 2.5$ is $(\Delta\nu)/\nu \times c \sim 1000 \text{ km s}^{-1}$ (where c is the speed of light). This means that the lines begin to overlap in frequency space at this redshift if the intrinsic full width zero intensity (FWZI) is larger than 1000 km s^{-1} . This is not the case in most of our sources, but potentially complicates the determination of the continuum redward of the C I(2–1) line. In the light of this we present conservative

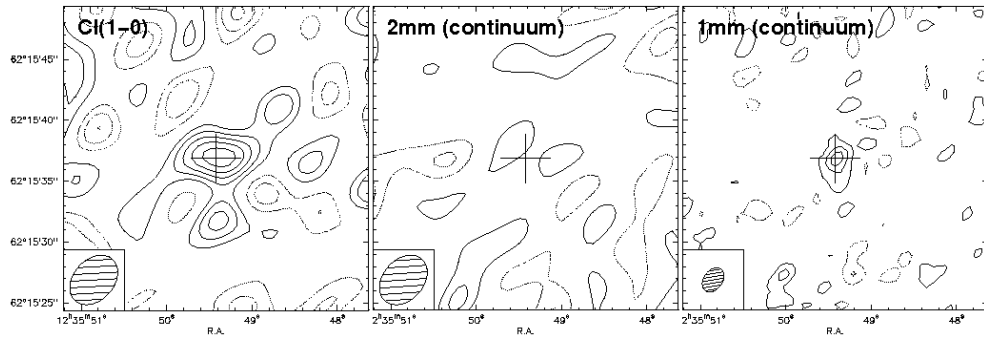


FIG. 4.— Results for SMM J123549+6215. *Left*: Integrated CI(1–0) emission from -400 km s^{-1} to $+400 \text{ km s}^{-1}$, with contours starting at $\pm 1\sigma$ in steps of 1σ ($1\sigma=0.26 \text{ mJy}$). *Middle*: Continuum measurement at 153.3 GHz (line-free channels of the CI(1–0) observations, using the same total bandwidth as for the line), same contouring and 1σ sensitivity as in the left panel. No continuum is detected at 153.3 GHz. *Right*: Continuum emission at 252.8 GHz, with contours starting at $\pm 2\sigma$ in steps of 2σ ($1\sigma=0.20 \text{ mJy}$). The beam sizes are shown in the bottom left corner, respectively (see Table 2).

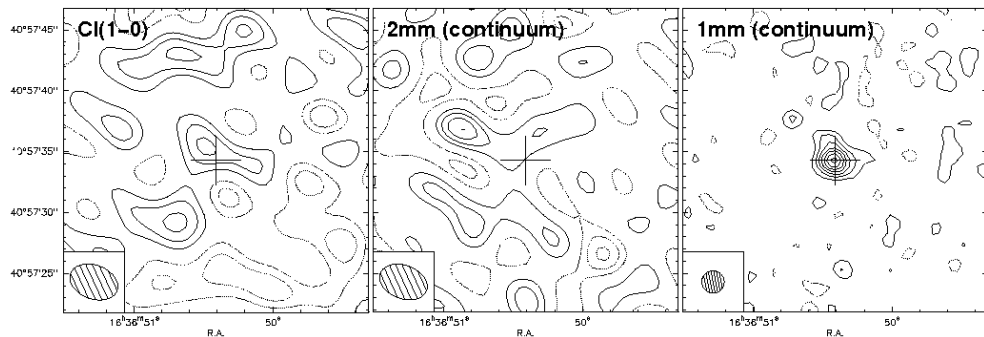


FIG. 5.— Results for SMM J163650+4057. *Left*: Integrated CI(1–0) emission from -500 km s^{-1} to $+500 \text{ km s}^{-1}$, with contours starting at $\pm 1\sigma$ in steps of 1σ ($1\sigma=0.24 \text{ mJy}$). The CI(1–0) line is not detected. *Middle*: Continuum measurement at 145.4 GHz (line-free channels of the CI(1–0) observations, using the same total bandwidth as for the line), same contouring and 1σ sensitivity as in the left panel. The continuum at 145.4 GHz is not detected. *Right*: Continuum emission at 239.1 GHz, with contours starting at $\pm 2\sigma$ in steps of 2σ ($1\sigma=0.22 \text{ mJy}$). The beam sizes are shown in the bottom left corner, respectively (see Table 2).

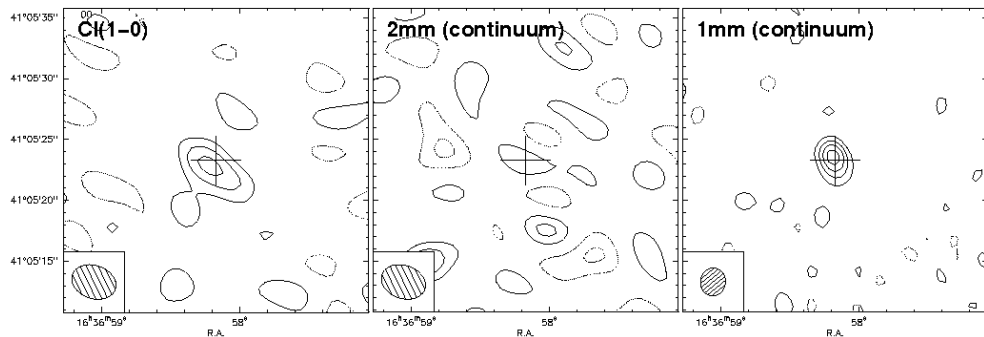


FIG. 6.— Results for SMM J163658+4105. *Left*: Integrated CI(1–0) emission from -400 km s^{-1} to $+200 \text{ km s}^{-1}$, with contours starting at $\pm 1.5\sigma$ in steps of 1.5σ ($1\sigma=0.29 \text{ mJy}$). *Middle*: Continuum measurement at 142.6 GHz (line-free channels of the CI(1–0) observations, using the same total bandwidth as for the line), same contouring and 1σ sensitivity as in the left panel. There is a tentative detection of the 142.6 GHz continuum in this source. *Right*: Continuum emission at 234.5 GHz, with contours starting at $\pm 2\sigma$ in steps of 2σ ($1\sigma=0.22 \text{ mJy}$). The beam sizes are shown in the bottom left corner, respectively (see Table 2).

5σ upper limits for the CI(2–1) line fluxes. For the 2 mm continuum we give 3σ upper limits. The σ 's used for deriving the upper limits are based on the 1σ noise in a channel that has the expected FWHM of the respective line.

3.1.2. Continuum Emission

Continuum emission at 1 mm has been detected in all cases (only one object is tentatively detected in the 2 mm band). We estimated the expected 1 mm and 2 mm continuum flux densities (for the respective frequency) based

on published SCUBA ($850 \mu\text{m}$) measurements of the individual sources (column 7 in Table 4), assuming a modified black body (see more detailed discussion in Section 4.2.2)⁵. We use the best-fit values for SMGs by Kovács et al. (2006, $T_{\text{dust,SMG}}=34.6\pm 3 \text{ K}$, $\beta_{\text{SMG}}=1.5$) and assign uncertainties of $\pm 10 \text{ K}$ to T_{dust} and ± 0.2 to β . In the case of the 1 mm observations, the measured flux densities of all our targets are consistent with these ex-

⁵ We derive almost identical estimates using an Arp 220 spectral energy distribution

TABLE 2
PLATEAU DE BURE OBSERVATIONS

source	FWZI ^a [km s ⁻¹]	CI trans.	ν_{obs} [GHz]	beamsize, P.A. " × ", °	rms ^b [mJy beam ⁻¹]	I _{CI} ^c [Jy km s ⁻¹]	S _{cont} ^d [mJy]	S _{exp} ^e [mJy]
SMM 02399–0136	~1000	CI(1–0)	129.2439	4.9×3.5, 161	0.11	1.9±0.2	<0.5	1.2±0.5
		CI(2–1)	212.5373	3.0×2.0, 165	0.18	1.8±0.9	6.2±0.2 ⁱ	7±3
SMM 123549+6215	~800	CI(1–0)	153.7041	4.6×3.3, 139	0.17	1.1±0.2	<0.8	0.8±0.3
		CI(2–1)	252.762	2.2×1.5, 145	0.20	<1.0	1.7±0.2	3.4±1.3
SMM 163650+4057	~1400	CI(1–0)	145.3946	4.1×2.8, 69	0.17	<0.7 ^f	<0.8	0.7±0.3
		CI(2–1)	239.0966	1.9×1.8, 99	0.18	<2.0	3.7±0.2 ^g	2.9±1.2
SMM 163658+4105	~1000	CI(1–0)	142.5726	3.7×2.8, 69	0.16	0.9±0.2	~0.6 ^h	0.8±0.3
		CI(2–1)	234.456	3.6×1.4, 174	0.21	<2.0	2.0±0.2	3.3±0.6

NOTE. — The uncertainties given here are only based on the formal fitting error and do not include the uncertainties in flux calibration (as discussed in Sec. 2.2).

^a The full width zero intensity (FWZI) has been estimated from published CO spectra (see references in Table 1).

^b Rms in mJy beam⁻¹ over the full 1 GHz bandwidth.

^c Upper limits to the CI(2–1) line fluxes are 5 σ values (see Section 3).

^d Measured continuum flux density at frequency given in column 4. In the case of non-detections we quote 3 σ upper limits.

^e Expected continuum at observed frequency based on SCUBA 850 μ m measurements (Table 4, Column 7) and assuming a modified blackbody with $\beta=1.5$ and a dust temperature of T=34.6 K (Kovács et al. 2006). The uncertainties reflect the model uncertainties of 40%, as discussed in Section 4.2.2.

^f Emission is marginally detected in the blue wing of the CO(3–2) line (Neri et al. 2003).

^g This source is potentially resolved in the continuum. The peak flux density is 2.8±0.2 mJy.

^h This source is only marginally detected in the 2 mm continuum (<3 σ).

TABLE 3
IRAM 30 M OBSERVATIONS

source	CI trans.	ν_{obs} [GHz]	rms ^a [mJy beam ⁻¹]	F _{peak} [mJy]	FWHM [km s ⁻¹]	I _{CI} [Jy km s ⁻¹]
APM 08279+5255	CI(2–1)	164.7988	1.6 (85 kms)	<4.8	—	<1.1 ^a
RX J0911+0551	CI(1–0)	129.6524	2.9 (40 kms)	13.3	140 ± 25	2.1±0.3
	CI(2–1)	213.2096	3.8 (45 kms)	14.8	145 ± 30	2.3±0.4
BRI 1335–0417	CI(1–0)	91.0229	4.8 (60 kms)	<14.6	—	<2.2 ^b
	CI(2–1)	149.6841	1.7 (60 kms)	<5.1	—	<0.8 ^b
SMM J14011+0252	CI(2–1)	227.0121	2.3 (50 kms)	14.4	205 ± 25	3.1±0.3
SMM J16359+6612	CI(1–0)	139.9229	0.8 (75 kms)	3.9,3.8	250, 160 ^c	1.7±0.3
	CI(2–1)	230.0991	0.9 (80 kms)	5.4,4.4	250, 160 ^c	2.2±0.3
PSS J2322+1944	CI(2–1)	158.0780	3.2 (60 kms)	8.0	160 ± 55	1.4±0.3

^a Velocity resolution for given rms shown in brackets.

^b 3 σ upper limit over the full width of the expected line width.

^c Profile fit with two Gaussian fits (e.g. Weiß et al. 2005a).

trapolations and inspection of individual datacubes did not reveal the presence of an additional CI(2–1) line. No significant continuum emission was detected in the 2 mm data, consistent with expectations (Table 2).

All derived line fluxes and continuum flux densities are summarized in Table 2. In the following we briefly discuss the individual sources.

3.1.3. SMM J02399–0136

This source is one of the first SMGs (S_{850 μ m}=26±3 mJy, Ivison et al. 1998) ever detected in CO emission ($J=3$, Frayer et al. 1998)⁶. It has subsequently been studied in detail in CO emission ($J=3$: Genzel et al. 2003, $J=1$: Ivison et al. 2010a). Ivison et al. (1998) noted that this source hosts a dusty AGN; its QSO lines are discussed in Villar-Martín et al. (1999) and Vernet & Cimatti (2001). In the $L_{\text{FIR}}-L_{\text{X-ray}}$ plane SMM J02399–0136 has the same luminosities as the Cloverleaf (Alexander et al. 2005a). Ivison et al. (2010b)

conclude that this source comprises a merger between a FIR-luminous starburst, a QSO host and a faint third component.

For our analysis we adopt a FWZI of ~1000 km s⁻¹ for SMM J02399–0136. The CI(1–0) line is clearly detected in both individual channel maps (Figure 1) and the integrated line emission (Figure 2, left). The total flux of the CI(1–0) line is 1.9±0.2 Jy km s⁻¹. The continuum at 2 mm is not detected at a 3 σ limit of S_{129 GHz} <0.51 mJy (Figure 2, middle). The source is clearly resolved in the 1 mm continuum at 212.5 GHz with a total flux density of S_{212 GHz}=6.2±0.2 mJy (Figure 2, right). Given the large linewidths in SMM J02399–0136 it is difficult to separate the continuum from possible CI(2–1) emission in this source at 1 mm wavelengths. Genzel et al. (2003) have derived a total continuum flux of 7.0±1.2 mJy measured at 235 GHz. If we assume that this is the correct continuum flux, we would expect a 212 GHz flux of ~4.9 mJy, or about 1.3 mJy less than what is observed. We conclude that some of the measured flux may be attributed

⁶ $J=3$: CO(3–2)

to C_I(2–1) emission in this source and derive a tentative C_I(2–1) flux of $\sim 1.8 \text{ Jy km s}^{-1}$ with a considerable error bar (50%). We note that SMM J02399–0136 is thought to be lensed (magnification factor $\mu=2.5$, Frayer et al. 1998, Genzel et al. 2003).

3.1.4. SMM J123549+6215

This source is sometimes also referred to as HDF 76 ($S_{850\mu\text{m}}=8.3\pm 2.5 \text{ mJy}$, Chapman et al. 2003) and has been detected in CO emission ($J=3$ and $J=6$: Tacconi et al. 2006, 2008, $J=1$: Ivison et al. 2010a). SMM J123549+6215 is X-ray bright (Alexander et al. 2005a) and its luminosity is classified as AGN-dominated (see also Alexander et al. 2005b, Takata et al. 2006).

We adopt a FWZI of $\sim 800 \text{ km s}^{-1}$ for SMM J123549+6215. The C_I(1–0) line is detected both in individual channel maps (Figure 3) and in the integrated line emission (Figure 4, left) with a total flux of $1.1\pm 0.21 \text{ Jy km s}^{-1}$. The continuum at 2 mm is not detected at a 3σ flux density limit of $S_{153 \text{ GHz}} < 0.78 \text{ mJy}$ (Figure 4, middle). The 1 mm continuum emission is detected at $S_{252.8 \text{ GHz}}=1.7\pm 0.2 \text{ mJy}$ (Figure 4, right). This is only marginally consistent with the tentative detection quoted by Tacconi et al. 2006 ($S_{213 \text{ GHz}}=2.0\pm 0.6 \text{ mJy}$, the extrapolated flux at 213 GHz would be $\sim 1 \text{ mJy}$), and within the expectations based on the extrapolation from the SCUBA measurement (Table 2). We derive a 5σ upper limit of the C_I(2–1) line (assuming a bandwidth of 800 km s^{-1}) of $< 1.0 \text{ Jy km s}^{-1}$.

3.1.5. SMM J163650+4057

This source is also known as Elias N2850.4 ($S_{850\mu\text{m}}=8.2\pm 1.7 \text{ mJy}$, Ivison et al. 2002) and first CO data ($J=3$ and $J=7$) have been presented by Neri et al. (2003)⁷ ($J=1$ data are shown in Ivison et al. 2010a). Improved CO data are shown in Tacconi et al. (2006, 2008, $J=3$ and $J=6$). The AGN broad lines of this source (which in fact is a pair of blue and red galaxies, Ivison et al. 2002) are discussed in Swinbank et al. (2005, see also Takata et al. 2006, Menéndez-Delmestre 2007, 2009).

The C_I(1–0) line is not detected in our data with a 3σ upper limit across the expected linewidth ($\sim 1000 \text{ km s}^{-1}$) of 0.7 Jy km s^{-1} (Figure 5, left, but see caption of Table 2). Likewise, the continuum at 2 mm is not detected at a 3σ flux density limit of $S_{145 \text{ GHz}} < 0.74 \text{ mJy}$ (Figure 5, middle). The 1 mm continuum emission appears to be slightly extended with $S_{239.1 \text{ GHz}}=3.7\pm 0.4 \text{ mJy}$ (peak flux: $2.8\pm 0.18 \text{ mJy}$, Figure 5, right), in rough agreement with our SCUBA extrapolation and with Neri et al. (2003) and Tacconi et al. (2006) who quote consistent 1 mm flux densities for this source ($S_{230 \text{ GHz}}=2.5\pm 0.4 \text{ mJy}$ and $2.6\pm 0.5 \text{ mJy}$, respectively). We derive a 5σ upper limit of the C_I(2–1) line (assuming a bandwidth of 1000 km s^{-1}) of $< 2.0 \text{ Jy km s}^{-1}$.

3.1.6. SMM J163658+4105

This source is also known as Elias N2850.2 ($S_{850\mu\text{m}}=10.7\pm 2.0 \text{ mJy}$, Ivison et al. 2002) and CO data

⁷ In Neri et al. (2003) this source is referred to as SMM J16368+4057

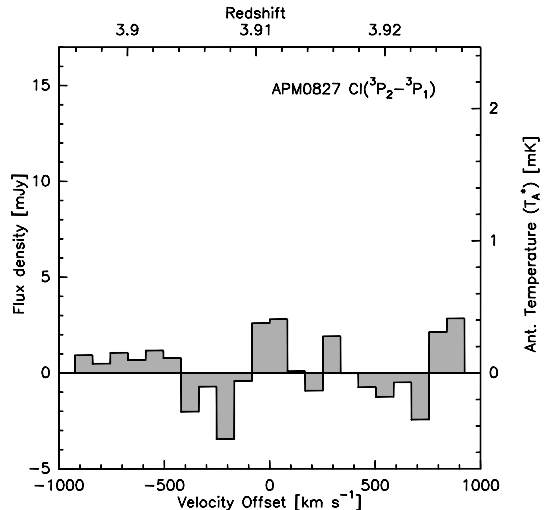


FIG. 7.— Left: C_I(2–1) spectrum of APM 08279+5255; the line is not detected.

are published in Greve et al. (2005, $J=3$)⁸, Tacconi et al. (2006, $J=3$ and $J=7$) and Ivison et al. 2010a ($J=1$).

The C_I(1–0) line is detected at $0.90\pm 0.18 \text{ Jy km s}^{-1}$ over a velocity width of 600 km s^{-1} (Figure 6, left). This is the only source in which the 2 mm continuum emission may be marginally detected at $S_{142.6 \text{ GHz}} \sim 0.6 \text{ mJy}$. If real (as suggested by the good match to the extrapolated SCUBA flux density, Table 2), the continuum emission would contribute $\sim 40\%$ to the C_I(1–0) flux density. Given the low S/N of the potential continuum flux, we do not apply this correction to the C_I(1–0) flux in the analysis that follows but note that such a correction would not change the statistical analysis below. The 1 mm continuum emission is detected at $S_{234 \text{ GHz}}=2.0\pm 0.22 \text{ mJy}$ (Figure 6, right), in good agreement with the extrapolation from the SCUBA measurement (and consistent with the estimate of Tacconi et al. 2006, of $S_{233 \text{ GHz}}=1.5\pm 0.5 \text{ mJy}$, their Table 1).

3.2. 30 m observations

We have observed both the C_I(1–0) and C_I(2–1) emission in 6 additional sources, four quasars and two submillimeter galaxies. All fitted parameters and line fluxes are summarized in Table 3. In the following we briefly discuss the individual sources.

3.2.1. APM 08279+5255

This source is one of the (apparently) brightest sources known to date, with a submillimeter flux of $S_{850\mu\text{m}}=75\pm 4 \text{ mJy}$ (Lewis et al. 1998). The first CO detections by Downes et al. (1999, $J=4$, $J=9$) already indicated the extreme excitation conditions of the molecular gas (studied in detail in Weiß et al. 2007). One of the explanations for its apparent brightness and extreme excitation is that the lensing geometry is such that the central 100 pc of this source is magnified by a large factor ($\mu=60\text{--}100$ Weiß et al. 2007, see also Egami et al. 2000)⁹. The C_I(1–0) line has been detected by Wagg et

⁸ In Greve et al. (2005) the source is referred to as SMM J16366+4105

⁹ We note that Riechers et al. 2009a derived a magnification factor of only ~ 4 for the molecular gas phase.

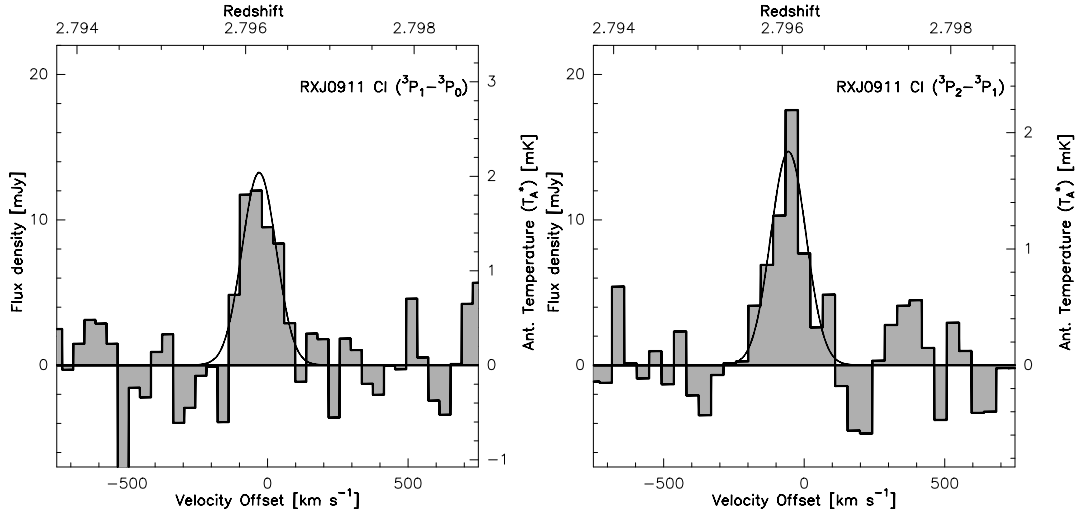


FIG. 8.— *Left*: CI(1–0) spectrum of RX J0911+0551. *Right*: CI(2–1) spectrum of RX J0911+0551. See Table 3 for respective fluxes and noise.

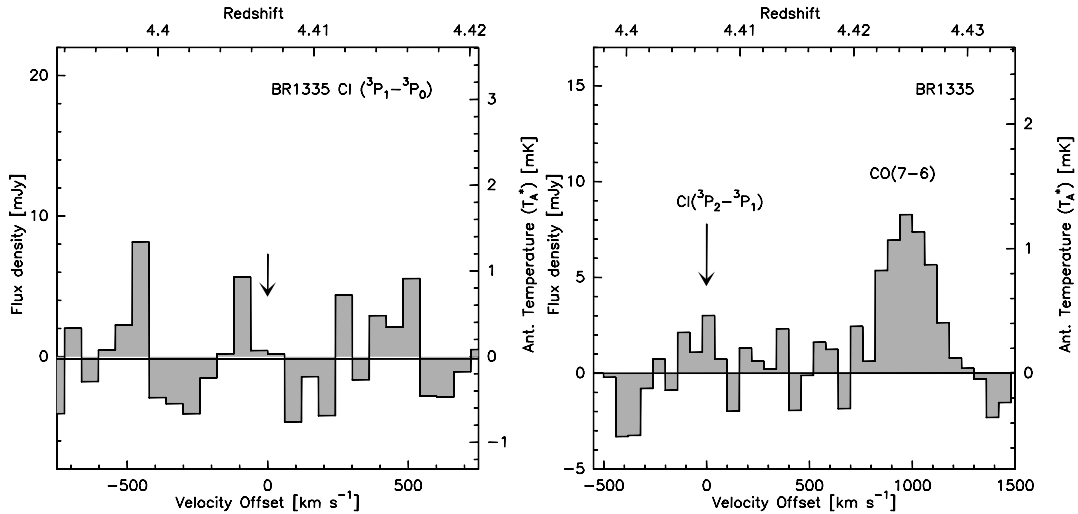


FIG. 9.— CI upper limits for BRI 1335–0417. *Left*: CI(1–0) observations. *Right*: CI(2–1) observations including the adjacent CO(7–6) line. The arrows in both panels indicate the expected central position of the CI lines.

al. (2006). The source is not detected in CI(2–1) emission with an upper limit of 1 Jy km s^{-1} (Figure 7, left; upper limits are given in Table 3).

3.2.2. RX J0911+0551

This source is bright in the submillimeter ($S_{850\mu\text{m}}=26.7\pm 1.4 \text{ mJy}$, Barvainis & Ivison 2002) and CO has been tentatively detected in this source by Hainline et al. (2004, $J=3$). Follow-up observations by W11 ($J=3,5,7,8,9$) show that the CO emission line is very narrow ($\text{FWHM}\sim 110 \text{ km s}^{-1}$). We detect both the CI(1–0) and CI(2–1) emission lines in this source (see Figure 8 and Table 3).

3.2.3. BRI 1335–0417

BRI 1335–0417 is bright in the submillimeter (e.g., Benford et al. 1999, we adopt $S_{850\mu\text{m}}=22\pm 4 \text{ mJy}$ from their Figure 2) and has first been detected in CO ($J=5$) by Guilloteau et al. (1997). High angular resolution

CO observations revealed a complex, possibly merging system (Carilli et al. 2002a, Riechers et al. 2008a, $J=2$). The source is not detected in both the CI(1–0) and CI(2–1) line with upper limits of 2.2 Jy km s^{-1} and 0.8 Jy km s^{-1} (Figure 9, right; see also Table 3). The spectrum of the CI(2–1) line in Figure 9 also includes the CO(7–6) line that is close in frequency space (the CO emission is discussed in W11).

3.2.4. SMM J14011+0252

SMM J14011+0252 is one of the first submillimeter galaxies ($S_{850\mu\text{m}}=15\pm 2 \text{ mJy}$, Ivison et al. 2000) that has been detected in CO emission (Frayer et al. 1999, $J=3$; Downes & Solomon 2003, $J=3, J=7$). Downes & Solomon argue that the source is strongly lensed, with a magnification factor $\mu=25\pm 5$. The CI(2–1) line is shown in Figure 10 (see also Table 3).

3.2.5. SMM J16359+6612

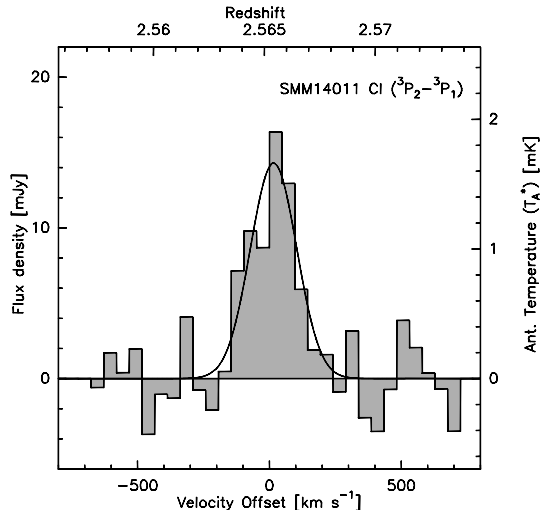


FIG. 10.— CI(2–1) spectrum of SMM J14011+0252. See Table 3 for fluxes and noise (see Weiß et al., 2005b, for the CI(1–0) spectrum of the same source).

This source is a triple–lensed system in which all three images are bright in the submillimeter (brightest image ‘B’: $S_{850\mu\text{m}}=17\pm 2\text{ mJy}$, Kneib et al. 2004). All images have subsequently been detected in CO emission (Sheth et al. 2004, $J=3$, Kneib et al. 2005, $J=3$). Kneib et al. (2004) have argued that the magnifications for the three images are 14 ± 2 , 22 ± 2 and 9 ± 2 , respectively. Higher– J CO transitions have been presented in Weiß et al. (2005a). The beams are $18''$ and $11''$ at our tuned frequencies at 2 mm and 1 mm respectively, i.e. only the brightest image (‘B’) is covered in our observations. In Figure 11 we show the CI(1–0) (left) and the CI(2–1) (right) spectra (see also Table 3).

3.2.6. PSS J2322+1944

PSS J2322+1944 is a lensed source ($\mu=5.4\pm 0.3$, Riechers et al. 2008b) which is bright in the submillimeter ($S_{850\mu\text{m}}=22.5\pm 2.5\text{ mJy}$, Isaak et al. 2002; $S_{1300\mu\text{m}}=9.6\pm 0.5\text{ mJy}$, Omont et al. 2001). Strong CO emission has been reported by Cox et al. (2002, $J=4$, $J=5$) and resolved imaging has revealed a molecular Einstein ring in this source by Carilli et al. (2002b, 2003, $J=2$) and Riechers et al. (2008b, $J=2$). The CI(1–0) line has been detected by Pety et al. (2004). We detect the CI(2–1) line at high significance (Table 3, Figure 12 shows a wider bandwidth spectrum after combining the CI(2–1) data with the CO(7–6) data presented in W11).

4. DISCUSSION

4.1. Previous high– z CI observations

We have observed CI emission in 10 high–redshift systems, targeting a total of 16 CI lines, and have detected a total of 10 lines (one more tentatively). In the discussion that follows we include CI measurements of high–redshift sources from the literature (an additional 7 sources). All CI measurements (including upper limits) to date are summarized in Table 4. We have re–calculated all line and far–infrared luminosities for the published sources to ensure that consistent assumptions and cosmological parameters are used in the analysis that follows.

4.2. CI, CO and FIR luminosities

4.2.1. Line luminosities

In the following we derive line luminosities both in units of L_{\odot} (L_{line}) and $\text{K km s}^{-1} \text{pc}^2$ (L'_{line}), where ‘line’ refers to either CO(3–2), CI(1–0) or CI(2–1). The former luminosity is given by

$$L_{\text{line}} = 1.04 \times 10^{-3} S_{\text{line}} \Delta v \nu_{\text{rest}} (1+z)^{-1} D_L^2, \quad (1)$$

(Solomon et al. 1992), where the luminosity of the line, L_{line} , is measured in L_{\odot} ; the velocity integrated flux, $S_{\text{line}} \Delta v$, in Jy km s^{-1} ; the rest frequency, $\nu_{\text{rest}} = \nu_{\text{obs}}(1+z)$, in GHz; and the luminosity distance, D_L , in Mpc (we have tabulated the luminosity distances in Table 5 assuming the cosmological parameters given at the end of Section 1). L_{line} (Eq. 1) is a true luminosity, i.e. it presents the amount of cooling that is radiated away by the respective line.

The line luminosity can also be expressed in units of $\text{K km s}^{-1} \text{pc}^2$:

$$L'_{\text{line}} = 3.25 \times 10^7 S_{\text{line}} \Delta v \nu_{\text{obs}}^{-2} D_L^2 (1+z)^{-3}. \quad (2)$$

(Solomon et al. 1992). As noted by Solomon & Vanden Bout (2005), as L'_{line} is proportional to the brightness temperature, the L' ratio of two lines is a measure of the ratio of their intrinsic brightness temperatures (assuming that both lines arise from the same volume, i.e. same area and linewidth).

We have calculated both luminosities for the CI(1–0), CI(2–1) and CO(3–2) lines and they are given in Table 5 (uncorrected for possible magnification).

4.2.2. Far–Infrared (FIR) luminosities

To derive consistent results within our sample, we have recalculated FIR luminosities for all sources based on their measured $850\mu\text{m}$ flux (as tabulated in Table 4). The reason why we chose the $850\mu\text{m}$ band as our reference wavelength is because continuum emission has been measured in this band for almost every source in our sample.

Following Blain et al. (2003), a simple description of the far–infrared SED as a function of frequency ν is based on a blackbody spectrum $B_{\nu} \sim \nu^3 / [\exp(h\nu/kT) - 1]$ at temperature T , modified by a frequency–dependent emissivity function $\epsilon_{\nu} \sim \nu^{\beta}$ (‘modified black body’). This yields a functional behavior at the source’s rest frame of $f_{\nu} \sim \nu^{3+\beta} / [\exp(h\nu/kT) - 1]$ (e.g. Blain et al. 2003).

At wavelengths where the dust is optically thin, the observed flux is proportional to the dust mass and the the observed flux density can be written as:

$$S_{\nu_o} = \frac{(1+z)}{D_L^2} M_{\text{dust}} \kappa(\nu_r) B_{\nu_r}(T_{\text{dust}})$$

(Downes et al. 1992), where $\kappa(\nu)$ is the dust absorption coefficient and the subscripts o and r refer to the observed and restframe frequencies.

We have derived FIR luminosities by integrating under a modified blackbody curve from 40 to $400\mu\text{m}$ (Sanders et al. 2003)¹⁰. The numbers are given in the last column in Table 5. For the quasars in our sample we have

¹⁰ The FIR luminosities decrease by 20–30% if the definition by

TABLE 4
 COMPILATION OF ALL HIGH-Z C I OBSERVATIONS TO DATE

source	z	magn. (μ)	$I_{\text{CO}(3-2)}$ [Jy km s ⁻¹]	$I_{\text{CI}(1-0)}$ [Jy km s ⁻¹]	$I_{\text{CI}(2-1)}$ [Jy km s ⁻¹]	$S_{850\mu\text{m}}$ [mJy]	references for columns ^a	[2]	[3]	[4]	[5]	[6]	[7]
[1]	[2]	[3]	[4]	[5]	[6]	[7]							
SMM J02399-0136	2.808	2.5	3.1±0.4	1.9±0.2	1.8±0.9	26±3	1,2	1,2	2		0	0	3
APM 08279+5255	3.911	60-100 ^b	2.2±0.2 ^c	0.93±0.13	<1.1	75±4 ^d	4	5	4		6	0	7,8
RX J0911+0551	2.796	~20	2.0±0.3 ^e	2.1±0.3	2.3±0.4	26.7±1.4	9,10	8	9,10		0	0	8
F10214	2.285	10 ^f	4.2±0.8	2.0±0.4	4.6±0.7 ^g	50±5	11	11	11		12,13	13	8
SDSS J1148+5251	6.419	1	0.18±0.04	—	0.22±0.05	7.8±0.7	14,15	—	15,16		—	17	18
SMM J123549+6215	2.202	1	1.6±0.2	1.1±0.2	<1.0	8.3±2.5	19,20	—	19,20		0	0	21
GN 20.2	4.051	1	0.5±0.2 ^c	—	<1.9 ^h	~9.9±2.3	22	23	22		—	24	25
GN 20	4.055	1	0.8±0.1 ^c	—	<1.2 ^h	20.3±2.1	22	23	22		—	24	25
BRI 1335-0417	4.407	1	1.0±0.2 ⁱ	< 2.2	<0.8	23±3 ^j	26	—	9		—	0	27
SMM J14011+0252	2.565	25±5 ^k	2.8±0.3	1.8±0.3	3.1±0.3	15±2	28,29	29	28,29		12	0	30
Cloverleaf	2.558	11 ^l	13.2±0.2	3.9±0.6	5.2±0.3	58.8±8.1	12	31	32		12,33	32	8
SMM J16359+6612	2.517 ^m	22±2	2.8±0.2	1.7±0.3	1.6±0.3	17±2	12,34,35	35	12,34,35		0	0	36
SMM J163650+4057	2.385	1	1.6±0.2	<0.72	<2.0	8.2±1.7	37,19,20	—	37,19,20		0	0	38
SMM J163658+4105	2.452	1	1.8±0.2	0.90±0.2	<2.0	10.7±2.0	39,19,20	—	37,19,20		0	0	38
MM 18423+5938	3.930	20 ⁿ	2.8 ± 0.3 ^c	2.3 ± 0.5	4.2 ± 0.8	70±5 ^o	40	—	40		40	40	40
SMM J213511-0102	2.326	32.5 ± 4.5	13.2 ± 0.1	16.0 ± 0.5	16.2 ± 0.6	113 ± 13	41	42	43		43	43	42
PSS J2322+1944	4.120	5.3±0.3	2.1±0.3 ^c	0.80±0.12	1.4±0.3	22.5±2.5	44	45	44		46	0	47

^a References in last column are the following papers: [0] this work; [1] Frayer et al. 1998; [2] Genzel et al. 2003; [3] Ivison et al. 1998; [4] Downes et al. 1999; [5] Weiß et al. 2007; [6] Wagg et al. 2006; [7] Lewis et al. 1998; [8] Barvainis & Ivison 2002; [9] W11; [10] Hainline et al. 2004; [11] Downes et al. 1995; [12] Weiß et al. 2005b; [13] Ao et al. 2008; [14] Bertoldi et al. 2003; [15] Walter et al. 2003; [16] Walter et al. 2004; [17] Riechers et al. 2009b; [18] Robson et al. 2004; [19] Tacconi et al. 2006; [20] Tacconi et al. 2008; [21] Chapman et al. 2003; [22] Daddi et al. 2009a; [23] Daddi et al. 2009b; [24] Casey et al. 2009; [25] Pope et al. 2006; [26] Guilloateau et al. 1997; [27] Benford et al. 1999; [28] Frayer et al. 1999; [29] Downes & Solomon 2003; [30] Ivison et al. 2000; [31] Venturini & Solomon 2003; [32] Weiß et al. 2003; [33] Barvainis et al. 1997; [34] Sheth et al. 2004; [35] Kneib et al. 2005; [36] Kneib et al. 2004; [37] Neri et al. 2003; [38] Ivison et al. 2002; [39] Greve et al. 2005; [40] Lestrade et al. 2010; [41] Swinbank et al. 2010; [42] Ivison et al. 2010; [43] Danielson et al. 2010; [44] Cox et al. 2002; [45] Riechers et al. 2008b; [46] Pety et al. 2004; [47] Isaak et al. 2002.

^b An average value of 80 is used for further analysis. See Riechers et al. (2009a) for a significantly lower μ for the CO emission.

^c No CO(3-2) measurements available. CO(3-2) fluxes have been derived from measured CO(4-3) fluxes assuming that the emission is thermalized up to $J=4$ (i.e., $S_{\text{CO}(3-2)} = (\frac{3}{4})^2 \times S_{\text{CO}(4-3)}$).

^d Barvainis & Ivison give $S_{850\mu\text{m}} = 84 \pm 3$ mJy.

^e Data from W11. Hainline et al. (2004) reported a significantly larger velocity width/total flux.

^f Downes et al. (1995) derive slightly different magnifications for the CO ($\mu=10$) and FIR ($\mu=13$) emission.

^g Consistent with the 2σ upper limit of 7 Jy km s⁻¹ given by Papadopoulos (2005).

^h 2σ upper limits by Casey et al. (2009).

ⁱ Extrapolated from the $J=5$ measurement by Guilloateau et al. (1997).

^j Value taken from Figure 2 of Benford et al. (1999).

^k Ivison et al. (2001) adopted a magnification value that is lower by an order of magnitude ($\mu=2.5$).

^l Kneib et al. (1998) give a magnification range of $\mu=18-30$.

^m Only the brightest component ('B') is covered here.

ⁿ Magnification factor unknown (Lestrade et al. 2010). We here assign a factor of 20 to this source; consistent with the large factors found for other strongly lensed SMGs.

^o The 850 micron flux is derived from the 1.2 mm flux given in Lestrade et al. 2010, assuming a modified black body with $T_{\text{dust}}=40$ K and $\beta=1.6$.

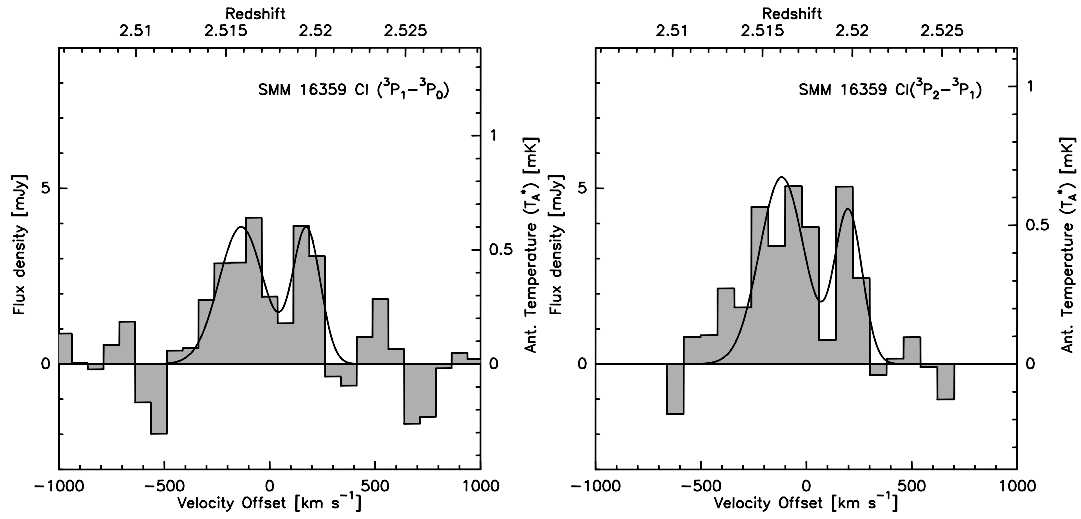


FIG. 11.— *Left*: CI(1-0) spectrum of SMM J16359+6612, *Right*: CI(2-1) spectrum of SMM J16359+6612. Two Gaussian functions have been fitted to account for the two components (e.g., Sheth et al. 2004, Kneib et al. 2005, Weiß et al. 2005a). See Table 3 for fluxes and noise.

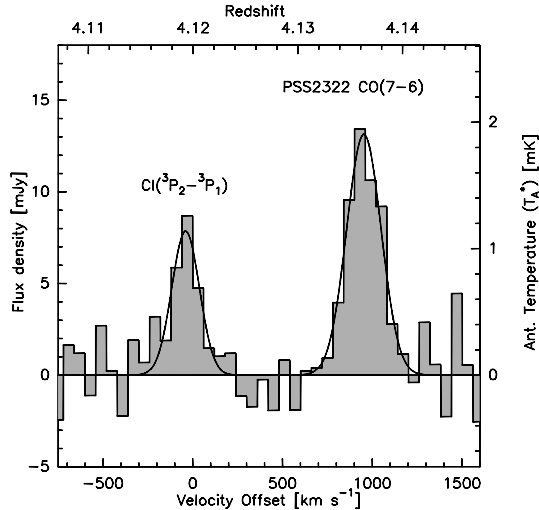


FIG. 12.— CI(2–1) spectrum of PSS 2322+1944 with the adjacent CO(7–6) line (W11). The velocity and redshift scales refer to the CI(2–1) observations. See Table 3 for fluxes and noise.

used the best-fit values ($T_{\text{dust}}=47\pm 3\text{ K}$, $\beta=1.6\pm 0.1$) derived by Beelen et al. (2006). Likewise, we have used the best-fit values by Kovács et al. (2006) for the SMGs ($T_{\text{dust}}=34.6\pm 3\text{ K}$, $\beta=1.5$). In both cases, following Beelen et al. (2006) and Kovács et al. (2006) we assign uncertainties of $\pm 3\text{ K}$ to T_{dust} and ± 0.1 to β . Based on this we assign uncertainties of $\Delta(\log L_{\text{FIR}})=0.15$, corresponding to $\sim 40\%$, to our FIR luminosity estimates (the measurement uncertainty in the $850\mu\text{m}$ fluxes is significantly lower than this number).

All luminosities given in Table 5 have *not* been corrected for magnification. To derive the unlensed luminosities, all numbers need to be divided by the respective magnification factors (μ) given in Table 4.

4.3. CI, CO and CI/CO line ratios

In Figure 13 we plot the CI(1–0) and CI(2–1) line luminosities as a function of CO(3–2) luminosities. Most CI luminosities are between 10% and 100% of the CO(3–2) luminosities (as indicated by the dashed diagonal lines). We calculate the $L'_{\text{CI}(1-0)}/L'_{\text{CO}(3-2)}$ ratios of all targets (Table 6). We chose the CO(3–2) transition as a measure for the CO luminosity as this transition has been observed for almost all targets. We find an average value of $L'_{\text{CI}(1-0)}/L'_{\text{CO}(3-2)}=0.32\pm 0.13$ with no significant differences between the QSO and SMG sample. We plot the $L'_{\text{CI}(1-0)}/L'_{\text{CO}(3-2)}$ ratios in Figure 14 as a function of $L_{\text{CI}(1-0)}/L_{\text{FIR}}$ (discussed in Section 4.7).

We now compare the $L'_{\text{CI}(1-0)}/L'_{\text{CO}(3-2)}$ ratios to systems at low-redshift (including our Galaxy). This comparison is complicated by a two facts: (a) in most low- z cases, the CO luminosity has been derived from the $J=1$ transition, not $J=3$ as in this study. We here assume $L'_{\text{CO}(1-0)}\approx 0.9\times L'_{\text{CO}(3-2)}$, Weiß et al. 2005a, Ao et al. 2008) – this translates to a $L'_{\text{CI}(1-0)}/L'_{\text{CO}(1-0)}=0.29\pm 0.12$ for the high-redshift sample; (b) The beam sizes of the CI(1–0) and CO observations are typically different for the low- z sources (this fact does not play a role at high redshift, where our beam sizes are in most cases larger than the source size).

Gerin & Phillips (2000) found an average value of $L'_{\text{CI}(1-0)}/L'_{\text{CO}(1-0)}=0.2\pm 0.2$ in nearby galaxies and similar values have been derived in other studies: e.g., M 83: 0.18 ± 0.04 , NGC 6946: 0.20 ± 0.04 (Israel & Baas 2001, their table 4), IC 342: 0.16 ± 0.03 , Maffei 2: 0.10 ± 0.05 (Israel & Baas 2003, their table 4), M 51: 0.22 ± 0.06 (Israel et al. 2006, their table 4), Hennize 2–10: 0.09 ± 0.03 , NGC 253: 0.22 ± 0.05 (Bayet et al. 2004, their tables 2 and 3), M 82: 0.2^{11} . The average of the same value in the Milky Way is around 0.15 ± 0.1 ; Fixsen et al. (1999) (0.09, Ojha et al. (2001): 0.08, Oka et al. (2005): ranging from 0.05–0.3).

We conclude that, to first order, the $L'_{\text{CI}(1-0)}/L'_{\text{CO}}$ ratio does not appear to vary strongly with either environment or redshift, from low-excitation environments like the Milky Way all the way to extreme starbursts in the early universe. This finding is in agreement with our earlier conclusion based on a significantly smaller sample (Weiß et al. 2005b).

4.4. Atomic Carbon Excitation Temperature

Some sources have now been detected in both CI lines and we can use their flux ratio to derive the carbon excitation temperature. As discussed in Schneider et al. (2003) the carbon excitation temperature in the local thermodynamic equilibrium (LTE) can be derived from the CI line ratio via the formula

$$T_{\text{ex}} = 38.8 \times \ln\left(\frac{2.11}{R}\right)^{-1}, \quad (3)$$

where $R=L'_{\text{CI}(2-1)}/L'_{\text{CI}(1-0)}$. This assumes that both carbon lines share the same excitation temperature and are optically thin. The latter assumption can be tested using the equations given in Schneider et al. (2003, their equations A.6 and A.7). Since these equations require knowledge of T_{ex} we assume here, as a first guess, $T_{\text{ex}}=T_{\text{dust}}$ (Sec. 4.2.2) and intrinsic source sizes of $r=1\text{ kpc}$. This yields optical depths for the CI(1–0) line between 0.05–0.3, justifying the use of equation 3. Larger source sizes, as discussed by Tacconi et al. (2008), will lead to even lower optical depths.

We summarize the derived excitation temperatures in Table 6 and find values between ~ 25 and $\sim 45\text{ K}$ with an average value of $29.1\pm 6.3\text{ K}$. Note that if we used these derived T_{ex} , the CI lines are still optically thin. In the local universe, the carbon excitation temperature could only be derived for a few objects to date (using the same method as employed here): M 82: $\sim 55\text{ K}$ (using the values given in Stutzki et al. 1997), NGC 253: $\sim 20\text{ K}$ (Bayet et al. 2004), Milky Way: 17.5 K (Fixsen et al. 1999). Herschel SPIRE FTS observations will soon provide measurements of both CI lines in a sample of nearby ULIRGS (Van der Werf et al. 2010).

4.5. Atomic Carbon Masses

We now derive the atomic carbon masses of our targets. As derived in Weiß et al. (2003, 2005b), the carbon mass can be calculated from the CI(1–0) line luminosity via:

¹¹ Using the CI(1–0) measurement from Stutzki et al. 1997 and the CO(1–0) data presented in Walter et al. 2002.

TABLE 5
DERIVED LUMINOSITIES BASED ON THE VALUES GIVEN IN TABLE 4.

source	D_L^a [Gpc]	$L_{\text{CI}(1-0)}^b$ [$10^7 L_\odot$]	$L_{\text{CI}(2-1)}^b$ [$10^7 L_\odot$]	$L_{\text{CO}(3-2)}^b$ [$10^7 L_\odot$]	$L'_{\text{CI}(1-0)}^c$ [$10^{10} \text{ K km s}^{-1} \text{ pc}^2$]	$L'_{\text{CI}(2-1)}^c$ [$10^{10} \text{ K km s}^{-1} \text{ pc}^2$]	$L'_{\text{CO}(3-2)}^c$ [$10^{10} \text{ K km s}^{-1} \text{ pc}^2$]	L_{FIR}^d $10^{13} L_\odot$
SMMJ02399-0136	23.84	14.5±1.5	22±11	17±2	3.8±0.4	1.3±0.7	12.6±1.6	1.41
APM08279+5255	35.55	12.3±1.7	<24	20.4±1.9	3.2±0.5	<1.4	15.4±1.4	9.45
RXJ0911+0551	23.72	16±2	29±4	10.7±1.4	4.2±0.6	1.7±0.3	8.1±1.1	3.81
F10214	18.53	10.9±1.9	40±6	16±3	2.9±0.5	2.4±0.4	12±2	7.58
SDSSJ1148+5251	63.79	...	10±2	3.6±0.8	...	0.60±0.14	2.7±0.6	0.87
SMMJ123549+6215	17.71	5.5±1.1	<8.2	5.6±0.7	1.5±0.3	<0.5	4.3±0.5	0.45
GN20.2	37.08	...	<44	5±2	...	<2.6	3.7±1.5	0.55
GN20	37.12	...	<28	7.8±1.0	...	<1.6	5.9±0.7	1.12
BRI1335-0417	40.99	<35	<21	11±2	<9.2	<1.2	8.5±1.7	2.78
SMMJ14011+0252	21.35	12±2	33±3	12.9±1.4	3.1±0.5	1.97±0.19	9.7±1.0	0.82
Cloverleaf	21.28	25±4	56±3	60.4±0.9	6.7±1.0	3.28±0.19	45.7±0.7	8.64
SMMJ16359+6612	20.86	10.8±1.9	23±3	12.5±0.9	2.8±0.5	1.35±0.18	9.4±0.7	0.93
SMMJ163650+4057	19.53	<4.2	<19	6.5±0.8	<1.1	<1.1	4.9±0.6	0.45
SMMJ163658+4105	20.21	5.5±1.1	<20	7.7±0.9	1.4±0.3	<1.2	5.8±0.6	0.58
MM18423+5938	35.76	30 ± 7	92 ± 17	26 ± 3	8.0 ± 1.7	5.4 ± 1.0	20 ± 2	3.84
SMMJ213511-0102	18.94	88 ± 3	147 ± 5	51.2 ± 0.4	23.2 ± 0.7	8.7 ± 0.3	38.7 ± 0.3	6.15
PSSJ2322+1944	37.83	11.5±1.7	33±7	21±3	3.0±0.5	1.9±0.4	16±2	2.78

NOTE. — All luminosities given in this table are *uncorrected* for lensing. To correct for gravitational magnification, all numbers have to be divided by μ given in Table 4, Column 3.

^a For $H_0 = 71 \text{ km s}^{-1} \text{ Mpc}^{-1}$, $\Omega_\Lambda = 0.73$ and $\Omega_m = 0.27$ (Spergel et al. 2003, 2007).

^b From Equation 1, all units in $10^7 L_\odot$.

^c From Equation 2, all units in $10^{10} \text{ K km s}^{-1} \text{ pc}^2$.

^d See discussion in Section 4.2.2.

TABLE 6
DERIVED PHYSICAL PROPERTIES.

source	T_{ex}^a [K]	M_{CI} [$10^7 M_\odot$]	M_{H_2} [$10^{10} M_\odot$]	$X[\text{C I}]/X[\text{H}_2]$ 10^{-5}	$L_{\text{CI}(1-0)}/L_{\text{FIR}}$ 10^{-6}	$L'_{\text{CI}(1-0)}/L'_{\text{CO}(3-2)}$	$L'_{\text{CI}(2-1)}/L'_{\text{CI}(1-0)}$
SMMJ02399-0136	21.6±6.3	2.0±0.2	4.0±0.5	8.1±1.4	10±4	0.30±0.05	0.35±0.18
APM08279+5255	30.00	0.050±0.007	0.154±0.014	5.4±0.9	1.3±0.6	0.21±0.03	<0.44
RXJ0911+0551	23.5±3.0	0.26±0.04	0.32±0.04	14±3	4.2±1.8	0.52±0.10	0.41±0.08
F10214	42.0±10.9	0.36±0.06	0.95±0.18	6.4±1.7	1.4±0.6	0.24±0.06	0.8±0.2
SDSSJ1148+5251	30.00	...	2.2±0.5
SMMJ123549+6215	30.00	1.8±0.3	3.4±0.4	9±2	12±5	0.34±0.08	<0.34
GN20.2	30.00	...	3.0±1.2
GN20	30.00	...	4.7±0.6
BRI1335-0417	30.00	<11	6.8±1.4	<28	<13	<1.1	<0.13
SMMJ14011+0252	32.4±5.2	0.15±0.03	0.31±0.03	8.2±1.6	14±6	0.32±0.06	0.64±0.12
Cloverleaf	26.7±3.0	0.76±0.12	3.32±0.05	3.8±0.6	2.9±1.3	0.15±0.02	0.49±0.08
SMMJ16359+6612	26.2±4.0	0.16±0.03	0.34±0.02	7.8±1.5	12±5	0.30±0.06	0.48±0.11
SMMJ163650+4057	30.00	<1.4	3.9±0.5	<5.8	<9	<0.22	<1.0
SMMJ163658+4105	30.00	1.8±0.4	4.6±0.5	6.4±1.5	9±4	0.25±0.06	<0.82
MM18423+5938	34.1 ± 8.8	0.5 ± 0.1	0.79 ± 0.08	11 ± 3	8 ± 4	0.41 ± 0.10	0.7 ± 0.2
SMMJ213511-0102	22.4 ± 0.6	0.91 ± 0.03	0.95 ± 0.01	15.9 ± 0.5	14 ± 6	0.60 ± 0.02	0.37 ± 0.02
PSSJ2322+1944	32.8±7.4	0.71±0.11	2.4±0.3	4.9±1.0	4.1±1.8	0.19±0.04	0.65±0.17

NOTE. — All masses given in this table are *corrected* for lensing using μ given in Table 4, Column 3.

^a See Section 4.4. A temperature of 30 K has been assumed for all objects for which T_{ex} could not be derived.

$$M_{\text{CI}} = 5.706 \times 10^{-4} Q(T_{\text{ex}}) \frac{1}{3} e^{23.6/T_{\text{ex}}} L'_{\text{CI}(1-0)} [M_\odot] \quad (4)$$

where $Q(T_{\text{ex}}) = 1 + 3e^{-T_1/T_{\text{ex}}} + 5e^{-T_2/T_{\text{ex}}}$ is the C I partition function. $T_1 = 23.6 \text{ K}$ and $T_2 = 62.5 \text{ K}$ are the energies above the ground state¹². The above equation assumes optically thin C I emission and that both carbon lines are in LTE.

Where available we use the excitation temperature derived in Section 4.4 above. For those sources where only

¹² In the case of J 1148+5251, for which only the C I(2-1) line was observed, we use the corresponding equation given in Weiß et al. 2005b

one carbon line has been measured we assume $T_{\text{ex}}=30 \text{ K}$. We note that the total neutral carbon mass is not a strong function of the assumed T_{ex} unless the excitation temperature is below 20 K (unlikely to be the case in our targets, see also Figure 2 in Weiß et al. 2005a) so the exact choice of T_{ex} is not critical for the derivation of C I masses.

For completeness, we also derive molecular gas (H_2) masses assuming the standard conversion factor for starburst environments that should be applicable for SMGs and QSOs ($\alpha_{\text{CO}}=M_{\text{gas}}/L'_{\text{CO}}=0.8 M_\odot (\text{K km s}^{-1} \text{ pc}^2)^{-1}$, Downes & Solomon 1998). We here assume that the $J=3$ line is slightly subthermally excited (i.e., $L'_{\text{CO}(3-2)}=0.9 \times L'_{\text{CO}(1-0)}$, e.g., Weiß et al. 2005a). The

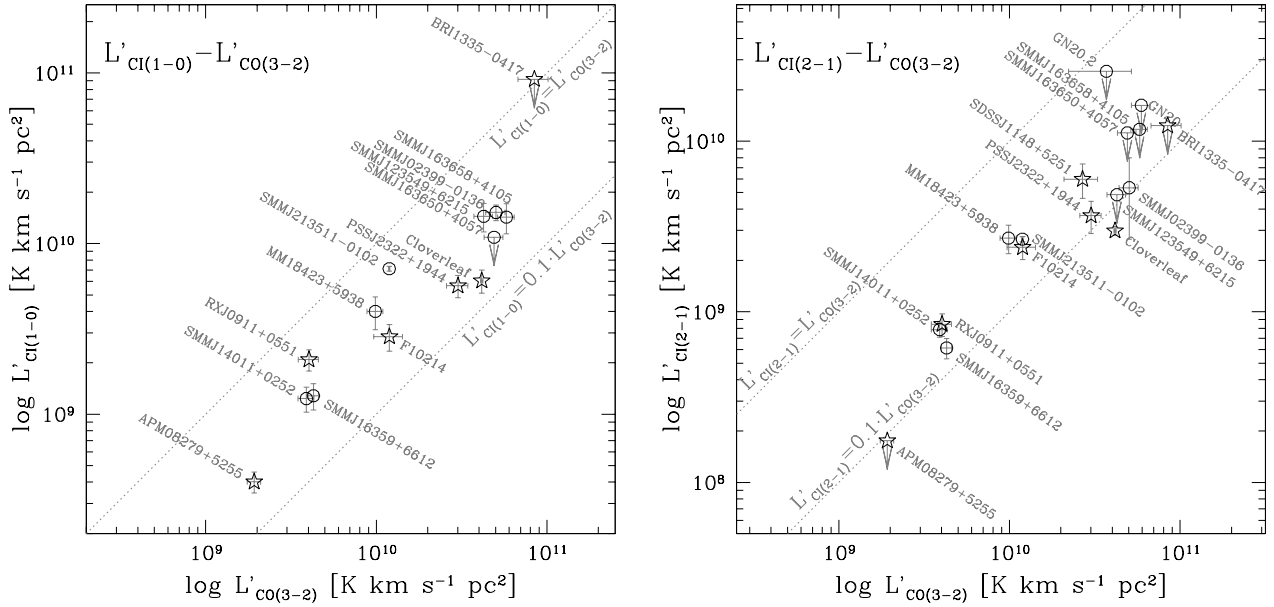


FIG. 13.— $L'_{\text{CI}(1-0)}$ (left) and $L'_{\text{CI}(2-1)}$ (right) as a function of $L'_{\text{CO}(3-2)}$ for all galaxies (stars indicate objects classified as quasars, circles: SMGs). The diagonal lines indicate $L'_{\text{CI}} = L'_{\text{CO}(3-2)}$ and $L'_{\text{CI}} = 0.1 \times L'_{\text{CO}(3-2)}$

CO luminosities (not corrected for magnification) are listed in Table 5, and the corresponding masses (here corrected for the magnification factors given in Table 4) in Table 6. We note that the molecular gas masses of the submillimeter galaxies would be higher by $\sim 50\%$ if we assumed the average $L'_{\text{CO}(3-2)} = 0.6 \times L'_{\text{CO}(1-0)}$ derived by Ivison et al. (2010a).

4.6. Atomic Carbon Abundances

We can now derive the atomic carbon abundance relative to H_2 via $X[\text{C I}]/X[\text{H}_2] = M(\text{C I})/(6M(\text{H}_2))$. The carbon abundance derived this way is independent of the magnification (ignoring potentially differential magnification) and the applied cosmology. We find a carbon abundance of $X[\text{C I}]/X[\text{H}_2] \approx 8.4 \pm 3.5 \times 10^{-5}$ for all sources (in agreement with earlier measurements by Ao et al., 2008, Weiß et al., 2005b). The carbon abundance for the SMGs would decrease if the 50% higher molecular gas masses implied by Ivison et al. (2010a) were used. For comparison, Frerking et al. (1989) have derived an abundance of up to 2.2×10^{-5} for high extinction regions in the Galactic star forming region Ophiuchus. Israel & Baas (2001, 2003) have estimated gas-phase abundances in nearby galaxies of order 4×10^{-4} (their Table 6). We conclude that the cold molecular gas (traced by C I and CO) is already substantially enriched in our sample galaxies at high redshift.

4.7. Cooling Contribution of Atomic Carbon

As noted by Pety et al. (2004), a comparison of the C I and FIR luminosities shows that the cooling by C I is negligible compared to the cooling by the dust continuum (average $L_{\text{C I}}/L_{\text{FIR}} \sim 10^{-5}$). In Figure 14 (left) we plot the $L'_{\text{CI}(1-0)}/L'_{\text{CO}(3-2)}$ ratio as a function of the cooling contribution of C I ($L_{\text{C I}}/L_{\text{FIR}}$). We here chose to plot

luminosity ratios to eliminate any uncertainties in magnification corrections (ignoring the possibility of differential magnification). Sources referred to as SMGs appear to have higher $L'_{\text{CI}(1-0)}/L'_{\text{FIR}}$ ratios than QSOs. However, part of this offset is due to our choice of dust temperatures (Section 4.2.2): the lower T_{dust} in the SMGs (compared to the QSO sample) leads to lower L_{FIR} for a given $S_{850\mu\text{m}}$ flux density, which in turn results in higher $L_{\text{CI}(1-0)}/L_{\text{FIR}}$ ratios. To stick more to observables, we also plot the ratio of $L_{\text{C I}}/L_{850\mu\text{m}}$ in the right panel of Figure 14 ($L_{850\mu\text{m}} = 4\pi D_L^2 \nu S_{850\mu\text{m}}$; $\nu = 352$ GHz). This is justified because for a given L_{FIR} , $L_{850\mu\text{m}}$ is, to first order, independent of redshift for $z > 2$ (e.g. Blain et al. 2002). We still find an offset (higher $L_{\text{C I}}/L_{850\mu\text{m}}$) for the SMGs. This can be partly explained by a significant contribution of the central AGN to L_{FIR} in the QSOs (e.g., discussion in Weiß et al., 2007a, for APM 08279+5255, the source with the lowest ratio in our study). An alternative explanation is that the cooling contribution of C I in the SMGs may be intrinsically higher than in the QSOs.

4.8. C I Ratios in the Context of PDR Models

The PDR models of Gerin & Phillips (2000) and our average ratio $L_{\text{C I}}/L_{\text{FIR}} \sim 10^{-5}$ suggest an average interstellar radiation field of order $10^3 \times G_0$ (where G_0 is the local Galactic interstellar ultraviolet radiation field). Such high radiation fields have also been derived for other high- z sources (e.g., Maiolino et al. 2005, Ivison et al. 2010b).

Our derived average C I(1-0)/C I(2-1) line ratio (in units of L') is 0.55 ± 0.15 which translates to a ratio of 2.7 ± 0.9 in units of line intensity (which scales as ν^3). For a $10^3 \times G_0$ radiation field, the PDR models by Kaufman et al. (1999, their figure 8) and Meijerink et al. (2007, their figure 3) imply low H_2 volume densities of order

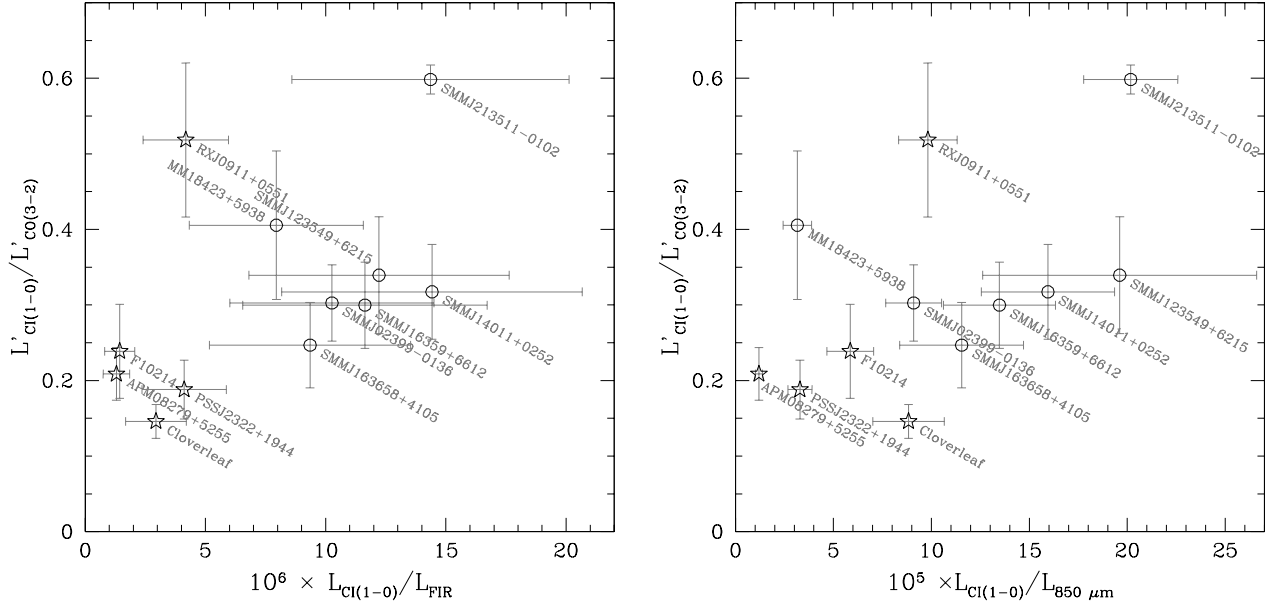


FIG. 14.— *Left:* $L'_{\text{CI}(1-0)}/L'_{\text{CO}(3-2)}$ ratio as a function of the cooling contribution of C I ($L_{\text{CI}}/L_{\text{FIR}}$). *Right:* Same $L'_{\text{CI}(1-0)}/L'_{\text{CO}(3-2)}$ ratio, this time plotted as a function of $L_{\text{CI}}/L_{850\mu\text{m}}$ to take out the FIR luminosity dependence on the assumed dust temperatures. SMGs are plotted as circles, QSOs as stars in both panels.

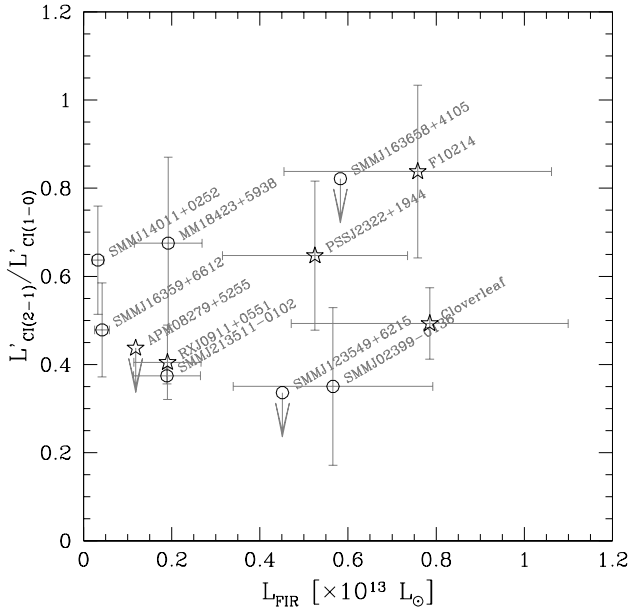


FIG. 15.— $L'_{\text{CI}(2-1)}/L'_{\text{CI}(1-0)}$ ratio as a function of FIR luminosity (corrected for lensing).

10^3 cm^{-3} . This density is of similar order as the critical density of both C I transitions which suggests that our derived excitation temperatures are, to first order, similar to the kinetic temperatures. Under this assumption, the average temperature of the C I lies in between the temperatures typically found in quiescent galactic regions (‘Cirrus-like’), 15–20 K, and those found in active starforming environments (50–60 K). This could imply that the interstellar medium traced by our C I observa-

tions is a mixture of a ‘cold’ and a ‘warm’ molecular gas component. We note however that the excitation temperature derived in equation 3 could be lower than the kinetic temperature if the C I excitation is not close to LTE.

The C I line ratios are not in agreement with the predictions by XDR models of Meijerink et al. (2007) which suggests that gas that is dominantly heated by an AGN should have a higher $\text{C I}(2-1)/\text{C I}(1-0)$ ratio than observed ($L'_{\text{CI}(2-1)}/L'_{\text{CI}(1-0)} > 0.8$, Fig. 3 in Meijerink). As shown in Figure 15 the C I ratio appears to be independent of the FIR luminosity and does not depend on the source type. Even in the case of APM 08279+5255, where the gas excitation is thought to be dominated by an AGN (Weiß et al. 2007), the $\text{C I}(2-1)/\text{C I}(1-0)$ ratio is lower than predicted for an XDR environment.

5. DISCUSSION AND CONCLUSIONS

We have presented new C I observations of 10 high-redshift galaxies. All systems that have been looked at in C I emission to date (including studies in the literature) are very bright emitters both in the submillimeter regime and in CO line emission, and many of them are lensed. Even so, individual detections of the C I lines have proven to be challenging with current instrumentation. In total, we have targeted 16 C I lines in this study, and have detected 10 of them. Including these new data, there are now a total of 17 sources in the literature in which C I has been observed (4 of which are not detected in neither the $\text{C I}(1-0)$ nor $\text{C I}(2-1)$ emission).

Our main finding is that the C I properties of high-redshift systems do not differ significantly from what is found in low-redshift systems, including the Milky Way. In addition, there are no major differences in C I properties between the QSO- and SMG-selected samples. We find that the $L'_{\text{CI}(1-0)}/L'_{\text{CO}}$ ratios (0.29 ± 0.12) are similar

to low- z galaxies (e.g., 0.2 ± 0.2 , Gerin & Phillips 2000).

Measurements of both C I lines offer the unique opportunity to constrain gas excitation temperatures of the molecular gas, independent of radiative transfer modeling. We derive an average carbon excitation temperature of 29.1 ± 6.3 K for our sample. This temperature is lower than what is typically found in starforming regions in the local universe despite the fact that the sample galaxies have star formation rate surface densities on kpc scales of 100's of $M_{\odot} \text{ yr}^{-1} \text{ kpc}^{-2}$ (comparable to the most extreme starbursts in the local universe, but on larger spatial scales). However, the temperatures are roughly consistent with published dust temperatures of high-redshift starforming galaxies (Beelen et al. 2006, Kovács et al., 2006, 2010). Low carbon excitation as well as dust temperatures could indicate that the measurements include a significant amount of gas/dust unaffected by star formation. However one should also keep in mind that the conversion of excitation temperature to kinetic temperature may be complicated by non-LTE excitation of atomic carbon.

The C I abundances in our sample galaxies ($X[\text{C I}]/X[\text{H}_2] = (8.4 \pm 3.5) \times 10^{-5}$) are comparable, within

the uncertainties, to what is found in local starforming environments (Section 4.6). This implies that the high- z galaxies studied here are significantly enriched in carbon on galactic scales, even though the look-back times are considerable (our average redshift of $z \sim 3$ corresponds to an age of the universe of ~ 2 Gyr).

In terms of the cooling budget the C I lines are a negligible coolant (average $L_{\text{C I}}/L_{\text{FIR}} = (7.7 \pm 4.6) \times 10^{-6}$). We find tentative evidence that this ratio may be elevated in the SMGs by a factor of a few compared to the QSOs, but a larger sample will be needed to beat down the current low-number statistics. The increase in sensitivity afforded by ALMA will be critical to increase the sample size and push C I studies at high redshift beyond the brightest systems that are accessible today.

We thank the referee for comments that helped to improve the paper and thank Rowin Meijerink for useful discussions. This work is based on observations with the IRAM Plateau de Bure Interferometer. IRAM is supported by INSU/CNRS (France), MPG (Germany) and IGN (Spain).

REFERENCES

- Alexander, D. M., Bauer, F. E., Chapman, S. C., Smail, I., Blain, A. W., Brandt, W. N., & Ivison, R. J. 2005a, *ApJ*, 632, 736
 Alexander, D. M., Smail, I., Bauer, F. E., Chapman, S. C., Blain, A. W., Brandt, W. N., & Ivison, R. J. 2005b, *Nature*, 434, 738
 Ao, Y., Weiß, A., Downes, D., Walter, F., Henkel, C., & Menten, K. M. 2008, *A&A*, 491, 747
 Barvainis, R., Maloney, P., Antonucci, R., & Alloin, D. 1997, *ApJ*, 484, 695
 Barvainis, R., & Ivison, R. 2002, *ApJ*, 571, 712
 Bayet, E., Gerin, M., Phillips, T. G., & Contursi, A. 2004, *A&A*, 427, 45
 Beelen, A., Cox, P., Benford, D. J., Dowell, C. D., Kovacs, A., Bertoldi, F., Omont, A., & Carilli, C. L. 2006, *ApJ*, 642, 694
 Benford, D. J., Cox, P., Omont, A., Phillips, T. G., & McMahon, R. G. 1999, *ApJ*, 518, L65
 Bertoldi, F., Cox, P., Neri, R., et al., 2003, *A&A*, 409, L47
 Blain, A. W., Smail, I., Ivison, R. J., Kneib, J.-P., & Frayer, D. T. 2002, *Phys. Rep.*, 369, 111
 Blain, A. W., Barnard, V. E., & Chapman, S. C. 2003, *MNRAS*, 338, 733
 Carilli, C. L., et al. 2002b, *ApJ*, 575, 145
 Carilli, C. L., et al. 2002a, *AJ*, 123, 1838
 Carilli, C. L., Lewis, G. F., Djorgovski, S. G., Mahabal, A., Cox, P., Bertoldi, F., & Omont, A. 2003, *Science*, 300, 773
 Casey, C. M., et al. 2009, *MNRAS*, 400, 670
 Chapman, S. C., et al. 2003, *ApJ*, 585, 57
 Cox, P., et al. 2002, *A&A*, 387, 406
 Daddi, E., Dannerbauer, H., Krips, M., Walter, F., Dickinson, M., Elbaz, D., & Morrison, G. E. 2009a, *ApJ*, 695, L176
 Daddi, E., et al. 2009b, *ApJ*, 694, 1517
 Danielson, A. L. R., et al. 2010, *MNRAS*, 1565
 Downes, D., Radford, J. E., Greve, A., Thum, C., Solomon, P. M., & Wink, J. E. 1992, *ApJ*, 398, L25
 Downes, D., Solomon, P. M., & Radford, S. J. E. 1995, *ApJ*, 453, L65
 Downes, D., & Solomon, P. M. 1998, *ApJ*, 507, 615
 Downes, D., Neri, R., Wiklind, T., Wilner, D. J., & Shaver, P. A. 1999, *ApJ*, 513, L1
 Downes, D., & Solomon, P. M. 2003, *ApJ*, 582, 37
 Egami, E., Neugebauer, G., Soifer, B. T., Matthews, K., Ressler, M., Becklin, E. E., Murphy, T. W., Jr., & Dale, D. A. 2000, *ApJ*, 535, 561
 Fixsen, D. J., Bennett, C. L., & Mather, J. C. 1999, *ApJ*, 526, 207
 Frayer, D. T., Ivison, R. J., Scoville, N. Z., Yun, M., Evans, A. S., Smail, I., Blain, A. W., & Kneib, J.-P. 1998, *ApJ*, 506, L7
 Frayer, D. T., et al. 1999, *ApJ*, 514, L13
 Frerking, M. A., Keene, J., Blake, G. A., & Phillips, T. G. 1989, *ApJ*, 344, 311
 Gerin, M. & Phillips, T. G., 1998, *ApJ* 509, L14
 Gerin, M. & Phillips, T. G., 2000, *ApJ* 537, 644
 Genzel, R., Baker, A., Tacconi, L., Lutz, D., et al., 2003, *ApJ*, 584, 633
 Greve, T. R., et al. 2005, *MNRAS*, 359, 1165
 Guilloteau, S., Omont, A., McMahon, R. G., Cox, P., & Petitjean, P. 1997, *A&A*, 328, L1
 Guilloteau, S., Omont, A., Cox, P., McMahon, R. G., & Petitjean, P. 1999, *A&A*, 349, 363
 Hainline, L. J., Scoville, N. Z., Yun, M. S., Hawkins, D. W., Frayer, D. T., & Isaak, K. G. 2004, *ApJ*, 609, 61
 Helou, G., Soifer, B. T., & Rowan-Robinson, M. 1985, *ApJ*, 298, L7
 Ikeda, M., Oka, T., Tatematsu, K., Sekimoto, Y., & Yamamoto, S. 2002, *ApJS*, 139, 467
 Isaak, K. G., Priddey, R. S., McMahon, R. G., Omont, A., Peroux, C., Sharp, R. G., & Withington, S. 2002, *MNRAS*, 329, 149
 Israel, F. P., & Baas, F. 2001, *A&A*, 371, 433
 Israel, F. P., & Baas, F. 2002, *A&A*, 383, 82
 Israel, F. P., & Baas, F. 2003, *A&A*, 404, 495
 Israel, F. P. 2005, *Ap&SS*, 295, 171
 Israel, F. P., Tilanus, R. P. J., & Baas, F. 2006, *A&A*, 445, 907
 Ivison, R. J., Smail, I., Le Borgne, J.-F., Blain, A. W., Kneib, J.-P., Bezecourt, J., Kerr, T. H., & Davies, J. K. 1998, *MNRAS*, 298, 583
 Ivison, R. J., Dunlop, J. S., Smail, I., Dey, A., Liu, M. C., & Graham, J. R. 2000, *ApJ*, 542, 27
 Ivison, R. J., Smail, I., Frayer, D. T., Kneib, J.-P., & Blain, A. W. 2001, *ApJ*, 561, L45
 Ivison, R. J., et al. 2002, *MNRAS*, 337, 1
 Ivison, R. J., Smail, I., Papadopoulos, P. P., Wold, I., Richard, J., Swinbank, A. M., Kneib, J.-P., & Owen, F. N. 2010b, *MNRAS*, 404, 198
 Ivison, R. J., Papadopoulos, P. P., Smail, I., Greve, T. R., Thomson, A. P., Xilouris, E. M., & Chapman, S. C. 2010a, *arXiv:1009.0749*
 Ivison, R. J., et al. 2010c, *A&A*, 518, L35
 Kaufman, M. J., Wolfire, M. G., Hollenbach, D. J., & Luhman, M. L. 1999, *ApJ*, 527, 795
 Kneib, J.-P., Alloin, D., Mellier, Y., Guilloteau, S., Barvainis, R., & Antonucci, R. 1998, *A&A*, 329, 827

- Kneib, J.-P., van der Werf, P. P., Kraiberg Knudsen, K., Smail, I., Blain, A., Frayer, D., Barnard, V., & Ivison, R. 2004, *MNRAS*, 349, 1211
- Kneib, J.-P., Neri, R., Smail, I., Blain, A., Sheth, K., van der Werf, P., & Knudsen, K. K. 2005, *A&A*, 434, 819
- Kovács, A., Chapman, S. C., Dowell, C. D., Blain, A. W., Ivison, R. J., Smail, I., & Phillips, T. G. 2006, *ApJ*, 650, 592
- Kovács, A., et al. 2010, *ApJ*, 717, 29
- Lestrade, J.-F., Combes, F., Salomé, P., Omont, A., Bertoldi, F., André, P., & Schneider, N. 2010, *A&A*, 522, L4
- Lewis, G. F., Chapman, S. C., Ibata, R. A., Irwin, M. J., & Totten, E. J. 1998, *ApJ*, 505, L1
- Maiolino, R., et al. 2005, *A&A*, 440, L51
- Meijerink, R., Spaans, M., & Israel, F. P. 2007, *A&A*, 461, 793
- Menéndez-Delmestre, K., et al. 2007, *ApJ*, 655, L65
- Menéndez-Delmestre, K., et al. 2009, *ApJ*, 699, 667
- Neri, R., Genzel, R., Ivison, R. J. et al. 2003, *ApJ*, 597, 113
- Ojha, R., Stark, A. A., Hsieh, H. H. et al. 2001, *ApJ*, 548, 253
- Oka, T., et al. 2005, *ApJ*, 623, 889
- Omont, A., Cox, P., Bertoldi, F., McMahon, R. G., Carilli, C., & Isaak, K. G. 2001, *A&A*, 374, 371
- Papadopoulos, P. P., Thi, W.-F., & Viti, S. 2004, *MNRAS*, 351, 147
- Papadopoulos, P. P. 2005, *ApJ*, 623, 763
- Pety, J., Beelen, A., Cox, P., Downes, D., Omont, A., Bertoldi, F., & Carilli, C. L. 2004, *A&A*, 428, L21
- Pope, A., et al. 2006, *MNRAS*, 370, 1185
- Riechers, D. A., Walter, F., Brewer, B. J., Carilli, C. L., Lewis, G. F., Bertoldi, F., & Cox, P. 2008b, *ApJ*, 686, 851
- Riechers, D. A., Walter, F., Carilli, C. L., Bertoldi, F., & Momjian, E. 2008a, *ApJ*, 686, L9
- Riechers, D. A., Walter, F., Carilli, C. L., & Lewis, G. F. 2009a, *ApJ*, 690, 463
- Riechers, D. A., et al. 2009b, *ApJ*, 703, 1338
- Robson, I., Priddey, R. S., Isaak, K. G., & McMahon, R. G. 2004, *MNRAS*, 351, L29
- Sanders, D. B., Mazzarella, J. M., Kim, D.-C., Surace, J. A., & Soifer, B. T. 2003, *AJ*, 126, 1607
- Schneider, N., Simon, R., Kramer, C., Kraemer, J., Stutzki, J., & Mookerjee, B. 2003, *A&A*, 406, 91
- Schöier, F. L., van der Tak, F. F. S., van Dishoeck, E. F., & Black, J. H. 2005, *A&A*, 432, 369
- Sheth, K., Blain, A. W., Kneib, J.-P., Frayer, D. T., van der Werf, P. P., & Knudsen, K. K. 2004, *ApJ*, 614, L5
- Solomon, P. M., Downes, D., & Radford, S. J. E. 1992, *ApJ*, 398, L29
- Solomon, P., Vanden Bout, P., 2005, *ARA&A*, 43, 677
- Spergel, D. N., et al. 2003, *ApJS*, 148, 175
- Spergel, D. N., et al. 2007, *ApJS*, 170, 377
- Stutzki, J., et al. 1997, *ApJ*, 477, L33
- Swinbank, A. M., et al. 2005, *MNRAS*, 359, 401
- Swinbank, A. M., et al. 2010, *Nature*, 464, 733
- Tacconi, L. J., Neri, R., Chapman, S. C. et al. 2006, *ApJ*, 640, 228
- Tacconi, L. J., et al. 2008, *ApJ*, 680, 246
- Takata, T., Sekiguchi, K., Smail, I., Chapman, S. C., Geach, J. E., Swinbank, A. M., Blain, A., & Ivison, R. J. 2006, *ApJ*, 651, 713
- Tielens, A. G. G. M., & Hollenbach, D. 1985a, *ApJ*, 291, 747
- Tielens, A. G. G. M., & Hollenbach, D. 1985b, *ApJ*, 291, 722
- Van der Werf, P. P., et al. 2010, *arXiv:1005.2877*
- Venturini, S., & Solomon, P. M. 2003, *ApJ*, 590, 740
- Vernet, J., & Cimatti, A. 2001, *A&A*, 380, 409
- Villar-Martín, M., Fosbury, R. A. E., Binette, L., Tadhunter, C. N., & Rocca-Volmerange, B. 1999, *A&A*, 351, 47
- Wagg, J., Wilner, D. J., Neri, R., Downes, D., & Wiklind, T. 2006, *ApJ*, 651, 46
- Walter, F., Weiß, A., & Scoville, N. 2002, *ApJ*, 580, L21
- Walter, F., Bertoldi, F., Carilli, C. L., et al. 2003, *Nature*, 424, 406
- Walter, F., Carilli, C., Bertoldi, F., Menten, K., Cox, P., Lo, K. Y., Fan, X., & Strauss, M. A. 2004, *ApJ*, 615, L17
- Weiß, A., Henkel, C., Downes, D., & Walter, F. 2003, *A&A*, 409, L41
- Weiß A., Downes, D., Henkel, C., Walter, F., 2005b, *A&A*, 429, L25
- Weiß A., Downes, D., Walter, F., Henkel, C. 2005a, *A&A*, 440, L45
- Weiß A., Downes, D., Neri, R., et al. 2007a, *A&A* 467, 955
- Weiß, A., Downes, D., Walter, F., & Henkel, C. 2007b, *From Z-Machines to ALMA: (Sub)Millimeter Spectroscopy of Galaxies*, 375, 25
- Weiß A., et al., 2011, in prep.
- White, G. J., Ellison, B., Claude, S., Dent, W. R. F. & Matheson, D. N., 1994, *A&A* 284, L23